

Title	Chemical functionalisation of silicon and germanium nanowires
Authors	Collins, Gillian;Holmes, Justin D.
Publication date	2011-06-03
Original Citation	Collins, G. and Holmes, J. D. (2011) 'Chemical functionalisation of silicon and germanium nanowires', Journal of Materials Chemistry, 21(30), pp. 11052-11069. doi: 10.1039/C1JM11028D
Type of publication	Article (peer-reviewed)
Link to publisher's version	<a href="http://pubs.rsc.org/en/content/articlelanding/2011/jm/c1jm11028d">http://pubs.rsc.org/en/content/articlelanding/2011/jm/c1jm11028d</a> - 10.1039/C1JM11028D
Rights	© The Royal Society of Chemistry 2011
Download date	2025-08-04 04:26:24
Item downloaded from	<a href="https://hdl.handle.net/10468/6764">https://hdl.handle.net/10468/6764</a>

# Chemical Functionalisation of Silicon and Germanium Nanowires

*Gillian Collins and Justin D. Holmes*

Materials and Supercritical Fluids Group, Department of Chemistry and the Tyndall National Institute, University College Cork, Cork, Ireland. Centre for Research on Adaptive Nanostructures and Nanodevices (CRANN), Trinity College Dublin, Dublin 2, Ireland.

\*To whom correspondence should be addressed: Tel: +353(0)21 4903608; Fax: +353 (0)21 4274097; E-mail: [j.holmes@ucc.ie](mailto:j.holmes@ucc.ie)

The reduced dimensionality of nanowires implies that surface effects significantly influence their properties, which has important implications for the fabrication of nano-devices such as field effect transistors, sensors and solar cells. This review will explore the strategies available for wet chemical functionalisation of silicon (Si) and germanium (Ge) nanowires. The stability and electrical properties of surface modified Si and Ge nanowires is explored. While this review will focus primarily on nanowire surfaces, much has been learned from work on planar substrates and differences between 2D and nanowire surfaces will be highlighted. The possibility of band gap engineering and controlling electronic characteristics through surface modification provides new opportunities for future nanowire based applications. Nano-sensing is emerging as a major application of modified Si nanowires and the progress these devices to date is discussed.

## 1. Introduction

Silicon (Si) and germanium (Ge) nanowires can be synthesised from a variety of techniques including those based on vapour-liquid solid<sup>1-4</sup>, solution-liquid-solid<sup>5-7</sup>, supercritical fluid-liquid-solid<sup>8-12</sup>, supercritical fluid-solid-solid<sup>13-15</sup> and oxide assisted growth<sup>16-18</sup> mechanisms.

While Si has become the material of choice for nanowire based devices, Ge remains a potentially attractive alternative for nanoscale applications due to its higher carrier mobility and larger exciton Bohr radius. There are two general approaches for modifying the surface of semiconductors; namely wet and dry chemical functionalisation. The latter method involves the formation of passivation layers in vacuo and has been well studied on planar Si and Ge surfaces. This review will not deal with dry functionalisation techniques and the reader is referred to excellent reviews concerning Si and Ge surface passivation under ultra-high vacuum conditions<sup>19-22</sup>. This review will present a broad overview of the synthetic approaches to chemical modification of Si and Ge nanowire surfaces. The oxidation characteristics of Si and Ge will firstly be discussed. The formation of hydrogen or halogen terminated surfaces are usually required to facilitate the grafting of organic molecules and so methods for the preparation of these surfaces will also be addressed. The latter part of the review will centre on the properties and applications of functionalised Si and Ge nanowires.

## **2. The Si/SiO<sub>2</sub> and Ge/GeO<sub>x</sub> Interfaces**

### *2.1 Oxidation Behaviour of Si Nanowires*

The oxidation behaviour of Si nanowires is dependent on a number of factors, such as oxidative conditions, growth direction and nanowire diameter. Dry furnace oxidation of Si nanowires at 920-950°C display reduced oxidation rates compared to planar Si, however, this oxidation behaviour is also dependent on the nanowire radius<sup>23</sup>. Nanowires with diameters > 44 nm were shown to exhibit oxidation rates comparable with bulk Si (~ 37 nm hr<sup>-1</sup>) but this rate reduces to 21 nm hr<sup>-1</sup> for a 5 nm diameter nanowire. The slower rate of oxidation was attributed to compressive stress normal to Si/SiO<sub>2</sub> interface, which arises from the greater volume of SiO<sub>2</sub> compared to Si. The effect of this compressive stress is more pronounced on

curved surfaces, resulting in a reduced oxide thickness for nanowires. Liu *et al.*<sup>24</sup> reported a similar trend for the dry oxidation of Si nanowires at 700°C and 900°C, and also observed that the presence of a chlorinated gas, trichloroethane (TCE) gave rise to a 60% and 25% increase in oxide thickness for nanowires oxidised at 700°C and 900°C, respectively. They further fabricated top-gated field effect transistors (FETs) using Si nanowires oxidised with or without the presence of TCE and observed significant hysteresis for nanowires oxidised at 700°C. Hysteresis-free devices could be fabricated from nanowires oxidised at 700°C in the presence of TCE, or at 900°C with or without the addition of TCE.

In contrast to furnace oxidation, rapid thermal oxidation of Si nanowires at 900 and 1000 °C, resulted in an initially enhanced oxidation rate, with nanowires possessing a ~50 % thicker oxide compared to planar Si substrates<sup>25</sup>. At longer oxidation times (>1 min) the oxidation rate of the nanowires and planar surfaces were found to be similar. Faster oxidation rates were attributed to tensile stress in the oxide which enhances the oxygen supply to the nanowire surface<sup>26</sup>. Shir *et al.*<sup>27</sup> studied dry oxidation of Si nanowires at 650-700 °C, in which the Au catalyst tips were removed by KI-I<sub>2</sub> treatment. An initial enhancement of the oxidation rate compared to planar Si was observed, followed by a much slower rate of oxidation for nanowires compared to planar Si.

Gösele and co-workers<sup>28</sup> found that the presence of Au greatly accelerated the rate of Si nanowire thermal oxidation, which is significant as Au is the most commonly employed catalyst in Si nanowire synthesis. Metal-enhanced oxidation of bulk Si has been known since the 1970's and for planar Si systems the SiO<sub>2</sub> oxidation layer reaches a saturated thickness, typically about twice the thickness of the Au layer<sup>29</sup>. Si nanowires display a different thermal oxidation behaviour; they undergo considerable oxidation along the nanowire axis while little or negligible radial oxidation is observed. Enhanced oxidation is thought to stem from Si atoms diffusing through the Au droplet and migrating to the surface where a reaction with

$O_2/H_2O$  can readily occur. Under dry oxidation conditions, the nanowire morphology is conserved as shown in figure 1<sup>30</sup>. In the presence of water, the rate of oxidation is greatly increased producing a lamella structured  $SiO_2$ , the nanowire adopts a bent morphology, or a bamboo-type structure, as illustrated in figure 1(d)<sup>30-31</sup>.

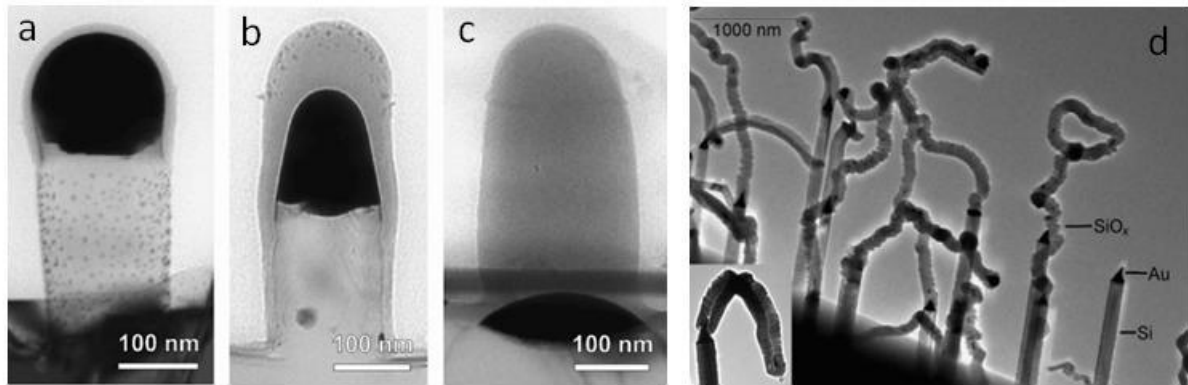


**Figure 1.** TEM images of Si nanowires oxidized at (a) 500°C, (b) 750°C and (c) 850°C, for 3 hr under dry conditions. (d) Air oxidation of Si nanowires at 250°C, for 4 h. The inset shows a back-bending  $SiO_x$  nanowire on top of a Si nanowire<sup>28,30</sup>. Figure 1 (a)-(c) reprinted with permission from reference 30. Copyright Institute of Physics. Figure (d) reprinted with permission from reference 28. Copyright Wiley-VCH.

## 2.2 Oxidation of Ge Nanowires

In contrast to Si, Ge displays more complex oxidation chemistry. Ge forms stable oxides in the 2+ ( $GeO$ ) and 4+ ( $GeO_2$ ), oxidation states, the latter of which is water soluble. Schmeisser<sup>32</sup> was the first to carry out synchrotron studies of oxidised Ge(100) and (111) surfaces and found the presence of all four Ge oxidation states. The oxidation behaviour of Ge is strongly dependant on the oxidative environment and is influenced by illumination conditions and crystal orientation<sup>33-34</sup>. Dry oxidation of planar Ge surfaces yields predominately  $Ge^{2+}$ , with minor amounts of  $Ge^{1+}$  and  $Ge^{3+}$  also present, while exposure to

ambient conditions results in a mixture of  $\text{Ge}^{2+}$  and  $\text{Ge}^{4+}$  oxides<sup>35</sup>. Hanrath and Korgel<sup>36</sup> observed that thermal annealing (300°C) of Ge nanowires produced predominately  $\text{Ge}^{1+}$ , in contrast to annealing of planar Ge(100) and (111) surfaces<sup>35</sup>, which yields mainly  $\text{Ge}^{2+}$ . Higher annealing temperatures (> 450°C) results in the desorption of GeO to produce an almost oxide-free surface<sup>35,37</sup> with some residual  $\text{Ge}^{3+}$  still present at 500°C.<sup>37</sup> The presence of water vapour greatly accelerates the rate of Ge oxidation<sup>38</sup>, as does exposure to UV light producing predominately  $\text{GeO}_2$ .<sup>39</sup> Prolonged ambient exposure (60 days) of Ge nanowires results in the disappearance of the  $\text{Ge}^{1+}$  oxidation state and the formation of a predominately  $\text{Ge}^{4+}$  oxide.<sup>40</sup> The oxidation behaviour of Ge nanowires is also dependent on the dopant type<sup>41</sup>; ambient exposure for 2 min after annealing of *p*-type Ge nanowires resulted in the rapid formation of GeO, followed by the slower formation of  $\text{GeO}_2$  over a few hours. For *n*-type Ge nanowires, air exposure resulted in the fast and immediate growth of  $\text{GeO}_2$ , which increased in thickness with further air exposure.

### 3. Hydrogen and Halogen Passivation of Si and Ge Nanowires

#### 3.1 Hydrogen Terminated Si and Ge Nanowires

Hydride termination of Si nanowires can be achieved by treatment with an aqueous HF solution. Fourier transform Infra-red (FTIR) spectroscopy of H-Si nanowires revealed a complex surface passivation with monohydride ( $\text{SiH}$ ), dihydride ( $\text{SiH}_2$ ) and trihydride ( $\text{SiH}_3$ ) species present. Based on vibrational frequencies reported for planar surfaces, Sun *et al.*<sup>42</sup> identified the presence of 3 monohydrides, corresponding to an ideal monohydride at 2085  $\text{cm}^{-1}$ , an adjacent adatom structure at 2070  $\text{cm}^{-1}$  and a monohydride at 2099  $\text{cm}^{-1}$ , observed at step defects on Si(111) surfaces. Similarly, using values reported for Si(100), relaxed dihydride and strained dihydride species were observed at 2102 and 2110  $\text{cm}^{-1}$ , respectively. A broad peak associated with trihydride species was also present, centred at 2137  $\text{cm}^{-1}$ .

Treatment of oxidised Ge nanowires with aqueous HF also yields a H-terminated surface. FTIR spectra of H-Ge nanowires exhibited a broad absorption peak at  $\sim 2010\text{ cm}^{-1}$ , associated with the  $\text{GeH}_x$  vibrations<sup>36</sup> consisting of mono-, di- and trihydride species<sup>43-44</sup>. The stability of the H-terminated Ge nanowires is dependent on the formation conditions, as observed by Adhikari *et al.*<sup>45</sup>, who reported that H-passivation of nanowires obtained from HF treatment oxidised faster than the H-passivation layer formed during nanowire synthesis by chemical vapour deposition (CVD); exhibiting more than a 4-fold increase in the oxide coverage after 18 min exposure in air. This difference in stability is most likely due to differences in the  $\text{GeH}_x$  conformations present at the nanowire surfaces.

### 3.2 Halogenated (Cl, Br, I) Si and Ge Surfaces

Halogen (Cl, Br, I) terminated Si surfaces can be prepared via a two step process, first by removing the surface oxide using aqueous HF, followed by treatment with an appropriate halogenation reagent. The preparation of chlorinated Si nanowires surfaces, often required for further organic functionalisation, can be achieved using saturated solutions of  $\text{PCl}_5$  in chlorobenzene heated to temperatures between  $80\text{--}100^\circ\text{C}$ <sup>46</sup>. The reaction can be mediated by a benzoyl peroxide radical initiator or by UV irradiation<sup>47-49</sup>. Halogenation of Ge surfaces can be readily achieved by treatment with aqueous halogenic acids (HCl, HBr, HI), which are effective in removing the surface oxide as well as terminating the nanowire surfaces with associated halogen atoms<sup>50</sup>. Halide-terminated Ge nanowires show greater ambient stability compared to H-terminated surface, with increasing molecular weight of the halogen species *i.e.*  $\text{Cl} < \text{Br} < \text{I}$ . After 24 h of ambient exposure, Cl-passivated Ge nanowires displayed considerable re-oxidation, Br-passivation showed minor re-growth of the oxide while I-terminated Ge nanowires remained oxide-free up to 48 hr of ambient exposure<sup>51</sup>.

## 4. Organic Functionalisation of Si and Ge Nanowires

Many reaction protocols to attach alkanes, alkenes and alkanethiols onto Si and Ge nanowires follow essentially the same procedure as those previously reported for 2D surfaces. Existing reviews by Bent<sup>52</sup>, Buriak<sup>53</sup> and Ciampi and co-workers<sup>54</sup> outline the mechanistic details of many of these reactions on planar Si and Ge surfaces. Nanowire surfaces are likely to share the same mechanistic particulars, so consequently these will not be discussed in detail in this review. Figure 2 outlines a schematic illustrating the various pathways for the preparation of alkylated, thiolated and arylated Si and Ge surfaces.

### 4.1 Alkylation of Silicon Nanowires

Hydrosilylation involves the incorporation of terminally unsaturated carbon-carbon bonds onto H-terminated Si surfaces. The reaction can be initiated thermally (150-200°C)<sup>55-58</sup>, photochemically (UV<sup>59-63</sup> or visible light<sup>64-65</sup>), through the presence of a Lewis acid catalyst<sup>66-67</sup> or a radical initiator<sup>55,68</sup>. An alternative approach to the formation of alkylated Si surfaces is via alkyl Grignard (R-MX<sub>2</sub>) reagents<sup>46,48,61,69-71</sup>. These precursors react with halogenated Si surfaces, typically Cl-terminated, however Grignard reagents have been shown to also attach via H-Si planar surfaces<sup>66</sup>. The functionalisation reaction is carried out at elevated temperatures (60-80 °C) and requires long reaction times (up to 8 days), particularly for Grignard reagents consisting of long alkyl chains. Bashouti *et al.*<sup>72</sup> functionalised Au-seeded Si nanowires with alkyl chains ranging from C<sub>1</sub>-C<sub>6</sub> through a chlorination/alkylation route and found that the chain length influenced the surface coverage, saturation time and oxidation resistance of the functionalised nanowires. The smaller van der Waal radius of C<sub>1</sub> groups (2.5 Å) compared to Si atomic separation distance (3.8 Å), facilitated a nearly full surface coverage for Si nanowires modified with methyl groups.

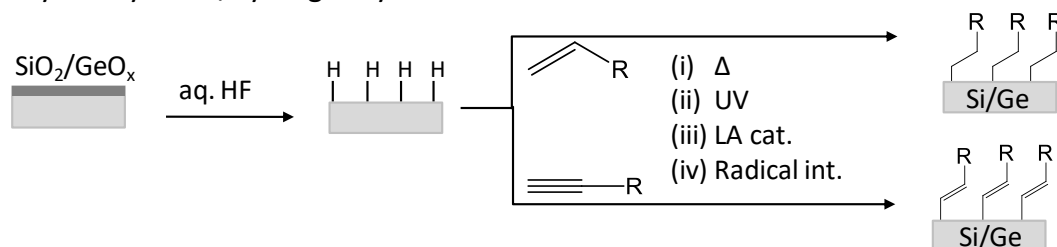


However as the chain length increased, the corresponding increase in the van der Waals radius restricts the packing of alkyl groups and limits maximum surface coverage to ~50-55%.

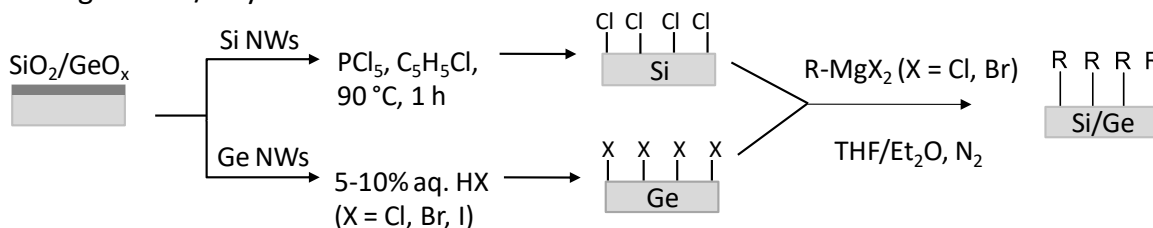
Assad *et al.*<sup>69</sup> compared the stability of methyl ( $\text{CH}_3$ ), propenyl ( $\text{CH}_3\text{-C}=\text{C-}$ ) and propynyl ( $\text{CH}_3\text{-C}\equiv\text{C-}$ ) terminated Si nanowires, prepared by chlorination/alkylation routes using the corresponding Grignard reagents. Both alkenyl and alkyne functionalisation layers exhibited high packing densities;  $103 \pm 5\%$  and  $97 \pm 5\%$ , respectively, relative to methyl termination. Stability studies of the modified nanowires showed that  $\text{CH}_3\text{-}$  and  $\text{CH}_3\text{-C}=\text{C-}$  functionalised surfaces were oxide-free up to 100 hr of ambient exposure, after which time the rate of oxidation of  $\text{CH}_3\text{-}$ terminated nanowires increased continuously with time. In contrast,  $\text{CH}_3\text{-C}=\text{C-Si}$  nanowires displayed an initial oxidation equivalent to  $\sim 0.12$  monolayers, but then stabilised on further ambient exposure. Si nanowires functionalised with  $\text{CH}_3\text{-C}\equiv\text{C-}$  exhibited the fastest rate of re-oxidation. The greater stability of the  $\text{C}=\text{C-Si}$  passivation layers was attributed to the  $\pi\text{-}\pi$  interactions of adjacent chains, which inhibits oxidation of the underlying Si atoms<sup>73</sup>. The formation of alkane and alkene monolayers via electrochemical grafting, and has been demonstrated on H-terminated Si nanowires<sup>74-75</sup>.

## Alkylation

### 1. Hydrosilylation/hydrogermylation



### 2. Halogenation/alkylation



## Thiolation



## Arylation

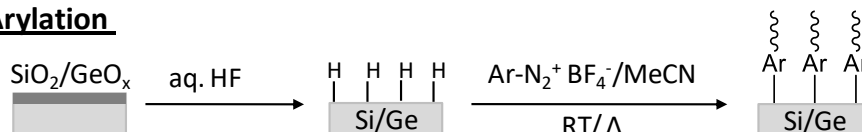


**Figure 2.** Schematic illustration various routes to Si and Ge nanowire functionalisation.

### 4.2 Alkylation and Thiolation of Germanium Surfaces

The first report of organic functionalisation of Ge surfaces was by Cullen and co-workers<sup>76</sup> in 1962, using gaseous HCl to prepare a Cl-terminated surface, followed by treatment with ethyl Grignard yielding an ethyl-passivated surface. There was little further investigation into the organic functionalisation of Ge surfaces until 1998 when He *et al.*<sup>77</sup> reported the alkylation of Ge(111) using a similar approach, however they utilised milder chlorination conditions using aqueous HCl, which did not cause surface roughness. Functionalisation of Ge nanowires via alkyl Grignard reagents is typically conducted from Cl-terminated surfaces<sup>36,78</sup> but the

reaction also proceeds effectively on Br and I-terminated Ge nanowires<sup>51</sup>. Analogous to hydrosilylation, hydrogermylation of alkenes and alkynes on H-terminated Ge nanowires produces alkyl and alkene functionalisation layers, respectively<sup>36,44,79</sup>. While alkylation produces a covalent Ge-C bond, reaction with 1-alkanethiols attach to the surface via a sulphur linkage (Ge-S) and yields highly oxidation resistant Ge surfaces. Grafting of thiols can be prepared from H-terminated<sup>36,78-80</sup> and halogenated-terminated (Cl, Br, I)<sup>51</sup> Ge nanowires. Holmberg and Korgel<sup>79</sup> found that alkyl monolayers, prepared via hydrogermylation, and thiol monolayers on Ge nanowires exhibited similar stability, except for exposure to highly oxidising conditions (30 % hydrogen peroxide), where the thiolated surfaces were less resistant to oxidation. In contrast, Ge nanowires alkylated by a halogenation/Grignard reagent route were less stable than thiolated nanowires<sup>51</sup>.

#### *4.3 Arenediazonium Salts as Precursors to Si and Ge Surface Modification*

Electrografting of arenediazonium salts has been used to prepare phenyl layers on H-terminated planar Si surfaces<sup>81-83</sup>. Stewart *et al.*<sup>84</sup> demonstrated the spontaneous grafting of organic ligands via arenediazonium salts on planar semiconductor surfaces such as Si and GaAs. The functionalisation procedure was carried out in anhydrous acetonitrile at room temperature, with reaction times of 1 hr resulting in successful covalent attachment of organic ligands to the Si surface. Haight and co-workers<sup>85</sup> observed that surface modification of Si nanowires could be achieved by exposing H-Si nanowires to a fine mist of the phenyl terpyridine diazonium solution.

Surface modification using arenediazonium salts has also been shown on Ge nanowires<sup>86</sup>. The thickness of the functionalisation layer was found to be influenced by the presence of aromatic ring substituents. Figure 3 (a) and (b) illustrates a TEM image of a Ge nanowire

modified using a nitrophenylbenzene diazonium salt ( $\text{NO}_2\text{Ph-BD}$ ). After a 2 hr reaction time the organic layer thickness was  $\sim 2$  nm, which increased to  $\sim 4$  nm after a 12 hr reaction time, as shown in figure 3(b). The formation of aryl multilayers is thought to proceed by the addition of aryl radicals<sup>84</sup>. Ge nanowires modified with 3,4,5-trifluorobenzene diazonium exhibit thin (1-2 nm) functionalisation layers, even after long immersion times (12 hr), as shown in figure 3(c). The formation of multilayers is hindered as the 3,4 and 5 ring positions block further aryl radical attack. Figures 3 (d) and (e) show the FTIR spectra for  $\text{NO}_2\text{Ph-BD}$  and  $\text{F}_3\text{-BD}$  functionalised Ge nanowires, respectively. Arenediazonium salts represent a versatile synthetic approach to attach aromatic ligands to Si and Ge nanowires.

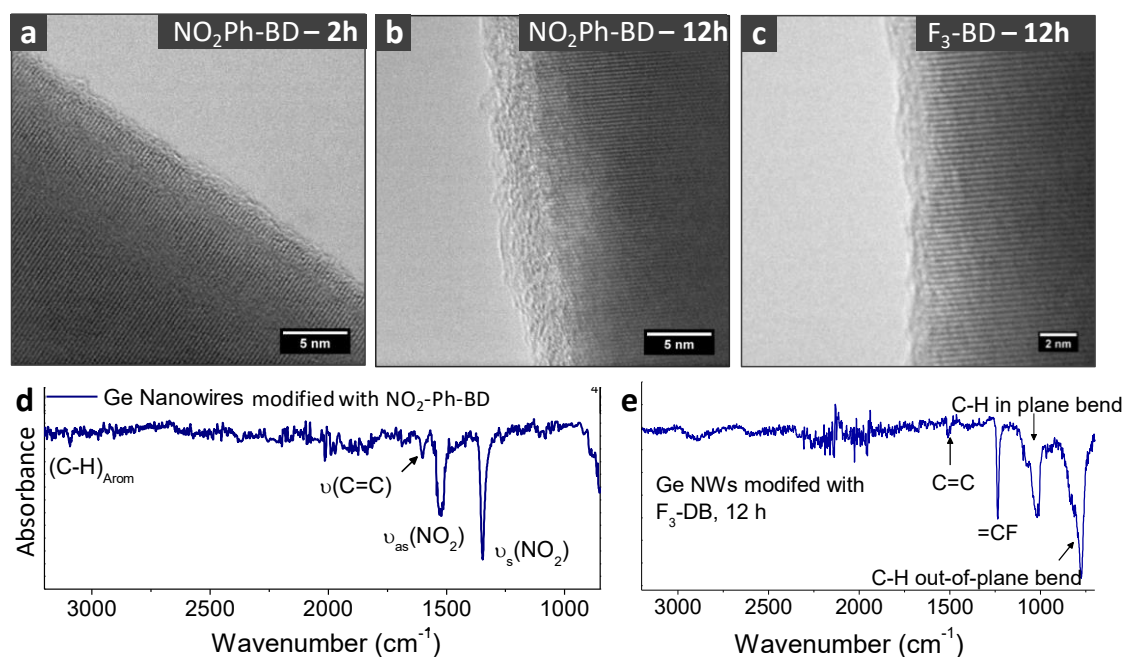


**Figure 3.** Functionalisation of Ge nanowires using arenediazonium salts. TEM images of Ge nanowires modified with  $\text{NO}_2\text{Ph-BD}$  for (a) 2 hr and (b) 12 hr. (c) TEM image of a Ge nanowire modified with  $\text{F}_3\text{-BD}$  for 12 hr. (d)-(e) FTIR spectra of functionalised Ge nanowires<sup>86</sup>. Reproduced with permission from reference 86. Copyright 2011, American Chemical Society.

#### 4.4 Modification and Extension of the Functionalisation Layer

Direct introduction of many functional groups onto H-Si and H-Ge surfaces is not possible as many bifunctional molecules will competitively react with the Si/Ge surface; for example, reaction with  $\omega$ -amino alkenes results in disordered monolayers as the amine and alkene moieties cross-react with the H-Si surface<sup>87</sup>. The introduction of the required functionality can be achieved by using protecting groups. Figure 4 illustrates the preparation of commonly employed protecting groups and the corresponding de-protection reactions. Amino groups can be introduced by using a *t*-butoxycarbonyl (*t*-Boc) protected amine<sup>88</sup>. Alternatively, phthalimide or acetamide moieties also serve as effective protecting groups for the introduction of well ordered amino functionalities<sup>87</sup>. Ester-terminated monolayers can be easily modified to obtain a variety of functional groups; reduction with NaBH<sub>4</sub> or LiAlH<sub>4</sub> results in alcohol termination, acid hydrolysis leads to carboxylic acid formation and reaction with alkyl Grignard reagents produces a tertiary alcohol<sup>56,61,89</sup>. Trifluoroacetyl groups are effective protecting agents for thiol groups<sup>90</sup>.

Protecting Groups for Amines	Deprotection	Protecting Groups for Thiols	Deprotection
	H <sup>+</sup> hydrolysis - 4 M HCl		10 % NH <sub>4</sub> OH
	Reflux in 5% hydrazine/ EtOH	<b>Protecting Groups for Carboxylic Acids</b>	
	(i) 25% TFA in methylene chloride (ii) 10% NH <sub>4</sub> OH		H <sup>+</sup> Hydrolysis
			Hydrolysis

**Figure 4.** Commonly used protecting groups for Si and Ge surface functionalisation

Click chemistry was first illustrated by Sharpless and co-workers and been widely used to introduce complex functionalities onto organically modified planar Si surfaces<sup>91</sup>. One of the most commonly used ‘click’ reactions used is the Cu(I) catalysed 1,3-dipolar cycloaddition of a terminal alkyne ( $C\equiv C$ ) and an organic azide ( $N_3^-$ )<sup>92</sup>. This reaction, commonly known as Huisgen coupling, introduces a 1,2,3-triazole group onto the functionalisation layer. The key to the Huisgen click reaction is the synthetic versatility, the reaction protocol can be applied to an extremely varied range of ligands. Suspène *et al.*<sup>93</sup> utilised this reaction to introduce electroactive thynyl-diphenylaniline (TPPA) groups onto Si nanowires. The coupling reaction usually requires long reaction times (>10 hr) when carried out at room temperature, however the use of microwave radiation can reduce the reaction time to < 30 min<sup>94</sup>.

Holmberg *et al.*<sup>95</sup> used carbodiimide coupling to attach amino-terminated (poly)ethylene glycol (PEG) to carboxylic acid groups on mercaptoundecanoic acid (MUA) functionalised Ge nanowires. Figure 5 illustrates the reaction scheme and TEM images of the modified nanowire surfaces. PEGylation of the nanowires allows for their dispersion in polar solvents such as DMSO and water, as shown in figure 5(c).

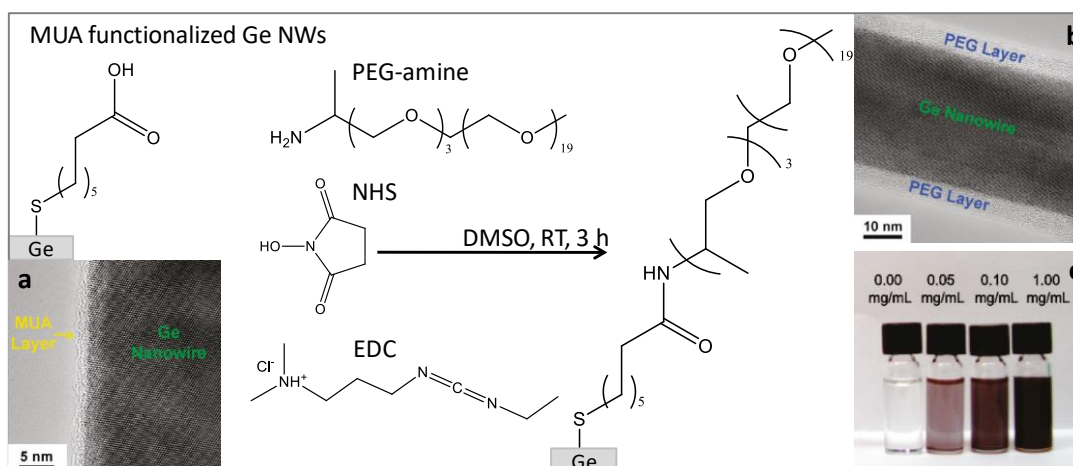


**Figure 5.** Reaction scheme for PEGylation of Ge nanowires by EDC coupling. TEM image of (a) mercaptoundecanoic acid and (b) PEG-functionalized Ge nanowire. (c) Photograph of PEGylated Ge nanowires dispersed in DMSO for 36 hr <sup>95</sup>. Reprinted with permission from reference 95. Copyright 2010, American Chemical Society.

Many complex molecules such as oligonucleotides cannot be attached directly to the nanowire surfaces and require the use of a bifunctional cross linker. The use of such molecules is essential in many sensing applications of nanowires (discussed in section 7). Gluteraldehyde is used to link amine species, for example a peptide chain, onto amine terminated nanowires, as illustrated in table 1(a). Maleimide activated surfaces are important for further reactivity with thiols groups, for example thiol-tagged DNA strains. Hydroxyl-terminated Si nanowires react with 3-maleimidopropionic-acid-*N*-hydroxy-succinimidester<sup>96</sup>, while amine terminated Si nanowires react with sulfo-succinimidyl 4-(*N*-maleimidomethyl) cyclohexene-1-carboxylate (SSMCC)<sup>97</sup>, as shown in table 1(b) and (c), respectively. Assad *et al.*<sup>69</sup> used a photoactive aryldiazirine cross linker, 4'-(3-trifluoromethyl-3*H*-diazirin-3-yl)-benzoic acid *N*-hydroxy-succinimide ester (TDBA-OSu), shown in table 1(d) to cross-link methyl terminated Si nanowires with amine groups. The use of this linker molecule is particular useful as it can covalently attach to methyl terminated Si nanowires, thus not requiring the need for the presence of a terminal heteroatom functional group at the nanowire surface. Furthermore, the photochemically induced reaction (365 nm) was complete after 15 min and an oxide-free Si surface was preserved.

**Table 1.** Bifunctional cross-linker molecules used for Si nanowire functionalisation.

	NW Functionalization	Cross-linker Molecule	Linking Functionality	Attachment Chemistry
a				
b				
c				
d				

Figure 5 depicts the reaction scheme used by Streifer *et al.*<sup>97</sup> to prepare DNA-modified Si nanowires and is a good illustration of how several strategies are required for surface modification. H-terminated Si nanowires were functionalised with a *t*-BOC protected amine by UV initiated hydrosilylation. Following deprotection, the amine terminated nanowires were reacted with the bifunctional linker SSMCC. Finally, the maleimido group was used to immobilise thiol-terminated DNA oligonucleotides onto Si nanowires.



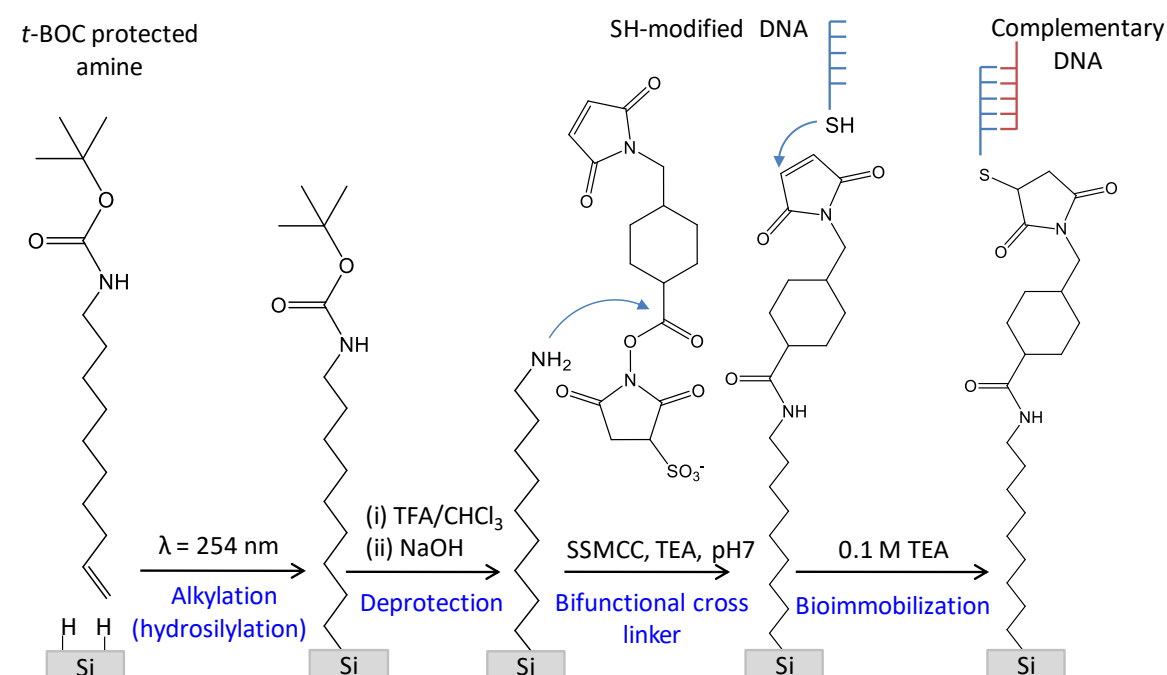


**Figure 5.** Reaction scheme used to prepare DNA functionalised Si nanowires<sup>97</sup>.

## 5. Properties of Functionalised Nanowires

### 5.1 Stability of Functionalised Nanowires versus Planar Surfaces

Si and Ge nanowires display many similar reactivity trends to their bulk counterparts, however it is evident from literature reports that functionalised nanowire and planar surfaces often exhibit different stabilities. Comparing the stability of modified nanowire and 2D surfaces is complicated by the fact that many synthesis methods produce nanowires with different growth directions<sup>77</sup>. Nanowires typically possess more than one surface facet, and can have different cross sectional geometries<sup>98-99</sup>. Furthermore, nanowire surfaces are more likely to be characterised by a higher concentration of defects such as stacking faults and twin defects, making direct quantitative comparison with planar surfaces challenging.

### 5.1.1 Stability Trends on Planar and Nanowire Si Surfaces

Sun *et al.*<sup>42</sup> observed that the FTIR spectra of H-terminated Si nanowires underwent negligible change when the nanowires were exposure to ambient conditions for 42 hr, in contrast to Si wafers which displayed limited stability on exposure to air. The increased stability of H-Si nanowires was also demonstrated by STM measurements of ultra thin (1-7 nm) Si nanowires, which were resistant to oxidation for several days on exposure to ambient conditions<sup>100</sup>. The stability exhibited by Si nanowires has been attributed to the high curvature, resulting in bending stress at the nanowire surface and consequently alters the structure of SiH<sub>2</sub> and SiH<sub>3</sub> phases, compared to bulk surfaces<sup>100-101</sup>. While H-Si nanowires display superior oxidation resistance on exposure to air, the same stability is not apparent under wet oxidation conditions, where Si nanowires oxidise rapidly. The poor water stability of H-Si surfaces has been attributed to the presence of OH<sup>-</sup> ions<sup>102</sup>.

Increased oxidation resistance of Si nanowires, relative to planar Si was also been observed for alkyl functionalised surfaces<sup>46</sup>. Si nanowires modified with alkyl chains ranging from C<sub>1</sub>-C<sub>10</sub>, via a chlorination/Grignard reagent process, exhibited SiO<sub>2</sub>/Si2p ratios ranging from 0.04-0.11 after 8 days of ambient exposure, compared to 0.15-0.18 for the corresponding 2D alkylated Si surfaces. The difference in stability was more pronounced for shorter alkyl chains; C<sub>1</sub>-Si nanowires exposed to air for 14 days displayed ~4 times less oxidation compared to 2D C<sub>1</sub>-Si. A 3-fold decrease in oxidation was observed for C<sub>2</sub>-modified surfaces, while (C<sub>3</sub>-C<sub>6</sub>)-functionalised nanowires only displayed marginally less oxidation than the 2D surfaces<sup>72</sup>. As well as increased stability, Si nanowires exhibited higher surface coverage and short reaction times to achieve maximum surface coverage relative to planar Si.

Haick *et al.*<sup>103</sup> compared the stability of methyl-functionalised Si nanowires having {100} surface facets with 2D Si(100) and observed that while the surface coverage was similar on

both substrates the nanowires exhibited stronger Si-C bonds compared to planar surfaces. Consequently, the nanowires displayed a 3-fold greater resistance to re-oxidation when exposed to ambient conditions. The Si nanowires also showed higher stability compared to 2D Si (111) surfaces, despite having a lower surface coverage. Haick and co-workers further observed the rate of alkylation to be greater for Si nanowires<sup>103</sup>. They attribute the increased stability and faster reaction kinetics to differences in the cohesive energy between nanowire and planar surfaces<sup>104</sup>.

#### *5.1.2 Stability Trends on Planar and Nanowire Ge Surfaces*

In contrast to H-Si nanowires, which possess superior stability in air, H-terminated Ge nanowires do not exhibit increased stability relative to 2D Ge<sup>105-106</sup> and oxidise only after a few minutes of ambient exposure<sup>36,45</sup>. However, organic functionalisation layers on Ge nanowires do possess greater stability than bulk Ge. Alkyl functionalised Ge(111) surfaces were found to be stable for up to 5 days<sup>77</sup>, while thiol-functionalised Ge(111) surfaces were only stable for 12 hr<sup>107</sup>. In contrast, alkylation by hydrogermylation and thiolation of Ge nanowires resulted in oxide-free surfaces up to 1 month of ambient exposure<sup>79</sup>. Furthermore, thiol passivation layers on Ge nanowires were observed to be more stable than monolayers prepared by Grignard reaction<sup>51,80</sup>, however the opposite trend was observed on planar surfaces. Interestingly, Ge nanowires functionalised with alkyl monolayers through hydrogermylation were found to display almost identical ambient stability to thiol monolayers<sup>79</sup>, indicating that the reduced stability of alkylation via a Grignard route may be attributed to the lower reactivity or poor alkyl packing achieved with alkyl Grignard reagents on Ge nanowire surfaces.

## 5.2 Electrical Properties of Functionalised Si and Ge Nanowires

Surface state depletion of charge carriers can result in considerable degradation in the electrical performance of semiconductor nanowires<sup>108-109</sup>. Kimukin *et al.*<sup>110</sup> found the surface charge density of Au-seeded Si nanowires to be  $\sim 2.6 \times 10 \text{ C cm}^{-2}$ , which is an order of magnitude greater than that for bulk Si. Interface states have been shown to effectively deplete an ultra thin (8 nm) Si nanowire, demonstrating the need for effective surface passivation<sup>111</sup>. Haick *et al.*<sup>112</sup> compared the electrical properties of oxidised, H-terminated and CH<sub>3</sub>-terminated Si nanowires and found that H-Si and CH<sub>3</sub>-Si nanowires exhibited a 4- and 7-fold increase in conductance, respectively, relative to oxidised Si nanowires. On exposure to air, the average conductance of H-modified nanowires continuously decreased with the mobility reduced from  $123 \text{ cm}^2 \text{ V}^{-1} \text{ s}^{-1}$  to  $87 \text{ cm}^2 \text{ V}^{-1} \text{ s}^{-1}$  after 672 hr of ambient exposure. The CH<sub>3</sub>-Si nanowires displayed an initial drop in mobility ( $140\text{-}124 \text{ cm}^2 \text{ V}^{-1} \text{ s}^{-1}$ ) but stabilised after 164 h exposure to air. On/off ratios greater than  $10^5$  were observed for CH<sub>3</sub>-terminated Si nanowires.

A later report by Haick and co-workers<sup>113</sup> investigated the electrical properties of Si nanowires field effect transistors (NW FET) functionalised by a range of organic functional groups, namely propyl alcohol, allyl, butyl and 1,3-dioxan-2-ethyl and observed interesting features in relation to the type of organic molecule attached to the nanowire surface. At a gate voltage ( $V_g$ ) = 0, and small-bias (drain-source voltage ( $V_{DS}$ )  $\sim 0 - 0.2 \text{ V}$ ) the trend in transconductance was in the order of propyl alcohol-Si < SiO<sub>2</sub>-Si < allyl-Si < butyl-Si < 1,3-dioxan-2-ethyl-Si, which correlates with the induced work function ( $\Delta\Phi$ ) of the organic molecule, *i.e.* a negative  $\Delta\Phi$  (propyl alcohol) resulted in an increase in the channel transconductance, while a positive  $\Delta\Phi$  (allyl-, butyl and 1,3-dioxan-2-ethyl) lead to a decrease in transconductance, relative to SiO<sub>2</sub>-Si nanowires. At large negative  $V_g$  ( $< -5 \text{ V}$ )

however, all functionalised nanowires exhibited lower transconductance ( $g$ ) values than oxidised Si nanowires, as shown in figure 6. Figure 6 further shows the significant improvement in the on/off ratios of functionalised Si nanowires compared to untreated nanowires.

Cui *et al.*<sup>114</sup> observed that functionalisation of oxidised Si surfaces with 4-nitrophenyloctadecanoate or tetraethylammonium bromide improved the conductance and on/off ratios of Si NW FETs. The effect of surface functionalisation was attributed to defect passivation and a reduction in trap states at the Si/SiO<sub>2</sub> interface. The work by Haick and Cui demonstrates that the electrical properties of nanowires are strongly influenced by the nature of passivating species not only covalently attached to the Si surface but also grafted onto the native oxide. Tuning the electrical properties of nanowires through surface modification and mechanisms of surface dominated transport in nanowires are discussed in further detail in section 6.2.

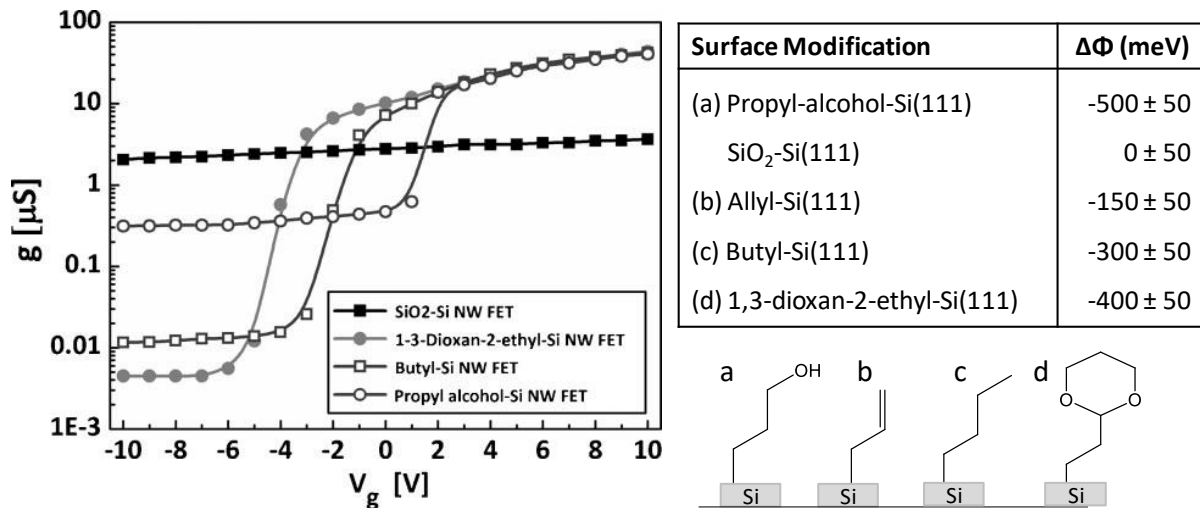


**Figure 6.** Transconductance ( $g$ ) versus back gate voltage ( $V_g$ ) for oxidised Si NW FETs and Si NW FETs modified with organic molecules (a)-(d). The table illustrates the change in the

work function  $\Delta\Phi$  on functionalised of Si(111) surfaces<sup>113</sup>. Reprinted with permission from reference 113. Copyright 2009, Wiley-VCH.

Unlike Si, the Ge/GeO<sub>x</sub> interface is characterised by a much higher density of surface defects, around 10<sup>13</sup> cm<sup>-2</sup> for bulk Ge, giving rise to poorer electrical properties compared to bulk Si<sup>115</sup>. Several groups have reported that non-functionalised, oxidised, Ge nanowires exhibit considerable hysteresis in their transport characteristics *i.e.* the drain-source current is not only dependent on the gate voltage but also the sweep direction<sup>41,78,116-117</sup>. Hysteresis has been attributed to charge trapping resulting from the presence of GeO<sub>x</sub> species and adsorbed water molecules. The influence of such surface states has been long recognised on bulk Ge<sup>118</sup>. Wang *et al.*<sup>41</sup> found the hysteresis behaviour of Ge NW FETs to be dependent on the dopant type. Brief air exposure of vacuum annealed (450°C, 0.5 hr) *p*-type NW FETs displayed no hysteresis, while *n*-type Ge NW FETs saw a reduction but not the complete removal of hysteresis. Furthermore, after exposure of *p*-type NW FETs to dry air and even pure oxygen the current versus gate voltage curves remained hysteresis free; indicating that the presence of adsorbed water molecules has a significant role on the electrical characteristics of Ge nanowires. The differing hysteresis behaviour can be attributed to the dopant dependent oxidation behaviour of Ge nanowires. As previously discussed in section 2.2, oxidation of *p*-type Ge nanowires initially forms GeO, while oxidation of *n*-type Ge nanowires results in the rapid formation of GeO<sub>2</sub>. Water molecules are more strongly associated with GeO<sub>2</sub> than GeO, consequently a *n*-type Ge NW FET possess more adsorbed water molecules that are difficult to remove under vacuum, resulting in the observed hysteresis trends.

An effective approach for improved electrical performance of Ge nanowires has been to remove the native  $\text{GeO}_x$  layer and replace it with an organic passivation layer to prevent the re-oxidation of the surface. Electrical characterisation of isoprene-functionalised Ge nanowires found that the presence of the organic passivation layer significantly improved carrier mobility relative to the non-passivated nanowires<sup>119</sup>. Hanrath and Korgel<sup>120</sup> observed that the Ge surface chemistry not only affected the transport properties but also influenced the contact properties. They found that alkane-functionalised Ge nanowires contacted with Pt electrodes, deposited by electron beam assisted CVD, displayed a contact resistance of  $\sim 0.8 \text{ M}\Omega$  and exhibited linear current-voltage (IV) characteristics. In contrast, untreated Ge nanowires displayed an increase in the contact resistance by 4 orders of magnitude, with the nanowires exhibiting non-linear IV behaviour and hysteresis at negative applied voltages.

## 6. Tunable Properties through Surface Functionalisation

### 6.1 Band Gap Engineering- Theoretical Predictions

Several groups have conducted theoretical calculations showing that the band gap of H-passivated  $\text{Si}^{121-126}$  and  $\text{Ge}^{121,127-129}$  nanowires increases with decreasing diameter, due to quantum confinement effects. The band gap is also strongly influenced by properties such as growth direction, surface facets and surface reconstruction<sup>122-123,130-135</sup>.

Density functional theory (DFT) calculations have shown a canted dihydride structure to be more energetically favourable than a symmetric dihydride structures, due to reduced H-H repulsion, on neighbouring  $-\text{SiH}_2$  groups<sup>136</sup>. Rotation of the dihydride groups further minimises the H-H repulsions in Si nanowires<sup>123</sup>. Titled Ge dihydrides have also be reported on  $\langle 110 \rangle$  orientated Ge nanowires<sup>135</sup>. DFTs calculations carried out by Xu *et al.*<sup>137</sup> showed that the electronic band gap of Si and Ge was sensitive to the conformational geometry of

surface hydrides; for  $\langle 110 \rangle$  Si nanowires, the presence of titled  $-\text{SiH}_3$  groups gave rise to an increase in the band gap energy relative to monohydride termination. Reconstructed H-terminated Si nanowires exhibit smaller band gaps due to strain introduced by surface reconstruction<sup>123</sup>.

Replacement of surface H-atoms with other passivating species can induce considerable changes in the band gap energy. Leu *et al.*<sup>138</sup> studied the effect of H, Cl, Br and I-passivation on the electronic band structure of Si nanowires using DFT calculations. Due to the formation of surface states associated with halogen binding, the band gap was found to follow increase in the order of  $\text{Cl} < \text{Br} < \text{I}$ , as shown in figure 7. For H-terminated nanowires, the relatively strong H-Si interactions resulted in the valance band (VB) maximum and conduction band (CB) minimum being concentrated in the nanowire interior<sup>139</sup>. On the other hand, the weaker bond strength of halogen atoms, cause the VB and CB states to spread out towards the nanowire surface. The effect of band gap reduction increases with higher surface coverage as the interaction between neighbouring halogen atoms further weaken the bonding to Si.

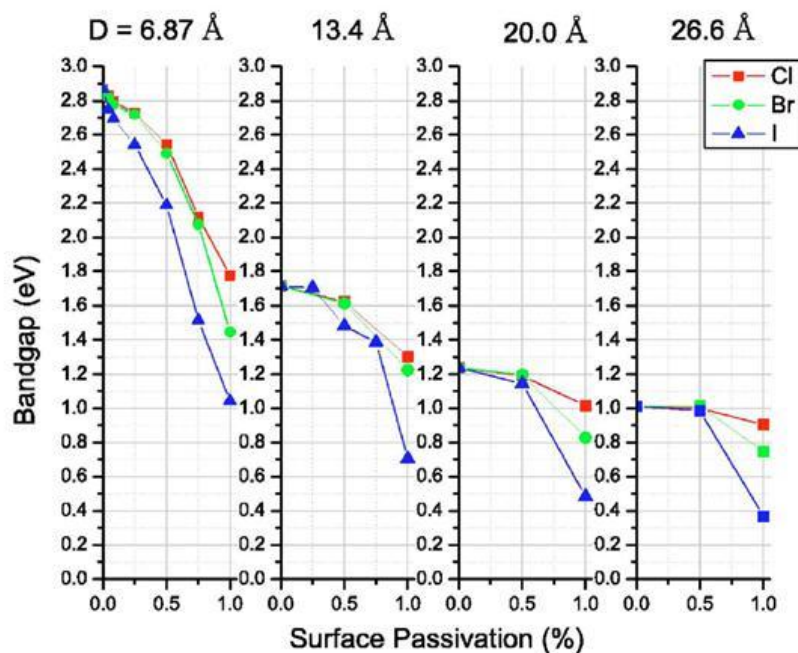




**Figure 7.** The change in band gap energy of H-Si nanowires as a function of halogen (Cl, Br, I) surface coverage<sup>138</sup>. Reproduced with permission from reference 138. Copyright 2006, American Physical Society.

Nolan *et al.*<sup>140</sup> investigated the effects of hydroxyl (-OH) and amine (-NH<sub>2</sub>) passivation on the band gap energy of ultra thin (~1 nm) Si(100) nanowires by DFT. Comparing nanowires of the same diameter, -OH and NH<sub>2</sub>- terminated nanowires exhibited a greater reduction in the band gap relative to H-passivated nanowires. The effect was greatest for -OH passivation, yielding a band gap 1.3 eV smaller than that of H-Si nanowires (2.6 eV). The band gap trend was attributed to competing effects of quantum confinement and the influence of hybridisation on the Si valence band (VB) edge. Interaction between the O/N 2*p* orbitals of -OH and -NH<sub>2</sub> passivated nanowires with the Si 3*p* increases the Si VB edge, resulting in the red-shift of the band gap relative to H-termination. Later studies found that the magnitude of the band gap reduction in -OH-terminated Si nanowires was also surface-facet dependent<sup>141</sup>. A 10 % reduction in the band gap was observed for {111} facets compared to 4 % on {100} surfaces, however, this value increased to 21 % on a (3 × 1) reconstructed surface. The growth direction dependence of the band gap for fully -OH and -F passivated Si nanowires are displayed in table 2 and show that nanowires with a <110> growth direction are the most sensitive to changes in band gap upon surface modification, while <111> orientated nanowires are the most resistant<sup>142</sup>. Another important effect of surface modification is that it can alter the nature of the band gap. When 50 % of H-terminations on a <100> Si nanowire are substituted for -OH or -F atoms, the band gap was predicted to change from a direct to indirect one<sup>142</sup>. No change in the nature of the band gap was predicted for <112> orientated -OH passivated Si nanowires<sup>143</sup>, however 50 % -F passivation was calculated to induce a transition from an indirect to direct band gap<sup>142</sup>. This result is

significant as the band gap of <112> H-Si nanowires have been shown to remain indirect even in the ultra thin diameter regime<sup>144-145</sup>.

Ng and co-workers<sup>146</sup> investigated the work function ( $\Phi$ ) of <110> Si nanowires and found  $\Phi$  to increase with decreasing diameter and to be dependent on surface passivation, following the trend of F-Si > H-Si > OH-Si. The trend in the  $\Phi$  is related to a change in the surface dipole upon chemical passivation<sup>147</sup>. The highly electronegativity of F atoms withdraw electrons from the Si surface, increasing  $\Phi$  relative to H-passivation. For –OH modification, two competing effects are present; while O is more electronegative than H, the –OH group is electron donating by resonance, dominating over the electronegativity effects, thereby lowering the  $\Phi$  relative to H-Si.

**Table 2.** Percentage reduction in band gap energy for differently oriented Si nanowires as a result of H-substitution with –OH and –F passivation.

Growth Direction	% Reduction in Band Gap relative to H-Si Nanowires	
	Fully -OH	Fully -F
<100>	24.4	38.3
<111>	18.5	22.2
<110>	36.3	54.8
<112>	39.3	30.2

Theoretical studies reported for passivated Ge nanowires remain scarce in the literature. Medaboina *et al.*<sup>127</sup> reported that removal of H-atoms from <111> Ge nanowires gives rise to electronic states in the band gap associated with the surface dangling bonds (SDB). In comparison to Si nanowires where SDB states occur deep in the band gap, Kagimura *et al.*<sup>148</sup> calculated shallow states for Ge nanowires. A similar trend in the band gap energy observed for non-H passivated Si nanowires was also seen for Ge nanowires, *i.e.* a red-shift in the band

gap with H-atom substitution. Ethine ( $\text{H-C}\equiv\text{C-}$ ) passivation of  $\langle 111 \rangle$  orientated Ge nanowires ( $d = 0.73 \text{ nm}$ ) resulted in an 18.2 % (1.82 eV) reduction in the band gap, compared to H-termination<sup>149</sup>. The reduced quantum confinement effects can be attributed to interaction of the  $\text{HC}_2$ -group with the Ge VB and conduction band (CB) edges, which is shown in figure 8 (c)-(d).

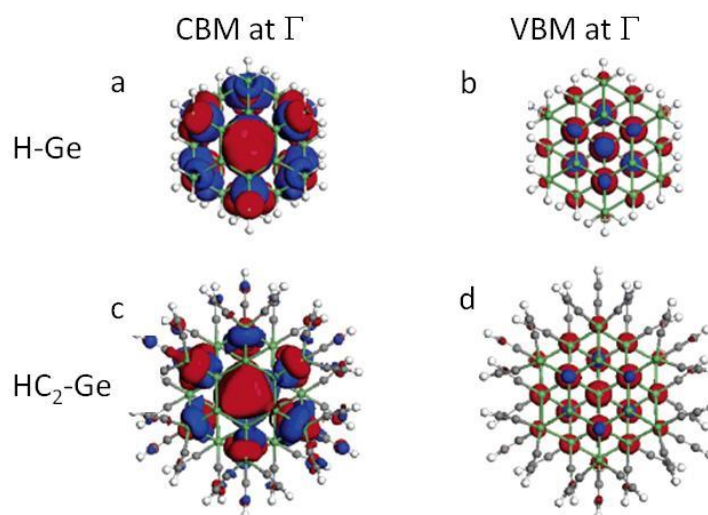


**Figure 8.** Wave functions for the conduction band maximum (CBM) and valence band maximum (VBM) at the  $\Gamma$  point of  $\langle 111 \rangle$  orientated (a)-(b) H-Ge nanowires and (c)-(d)  $\text{HC}_2$ -Ge nanowires. The red and blue areas represent the positive and negative regions, respectively<sup>149</sup>. Reprinted with permission from reference 149. Copyright 2006, American Chemical Society.

## 6.2 Surface Dominated Transport Properties and Molecular Doping

The extremely high surface area to volume ratio of nanowires implies that surface-dominated processes play a significant role in determining the transport properties of nanowires and allows the possibility of surface charge transfer doping as an alternative to conventional impurity doping strategies<sup>150</sup>. Jie *et al.*<sup>151</sup> studied the transport properties of H-passivated Si nanowires prepared by metal-assisted chemical etching of Si wafers and found the resistivity of  $p$ -type nanowires to be lower ( $\sim 2.2 \Omega$ ) than the original wafer ( $8\text{-}13 \Omega$ ) and decrease with

decreasing diameter. The hole concentration was found to decrease from  $4.2 \times 10^{16} \text{ cm}^{-3}$  in air to  $3.2 \times 10^{16}$  in vacuum, while the hole mobility increased from  $80 \text{ cm}^2 \text{ V}^{-1} \text{ s}^{-2}$  in air to  $170 \text{ cm}^2 \text{ V}^{-1} \text{ s}^{-2}$  in vacuum. The authors propose a mechanism whereby the presence of adsorbed water molecules would trap electrons from the nanowires to form  $\text{OH}^-$  ions. The presence of these negative surface charges gives rise to band bending and hole accumulation in the VB and consequently the observed conductivity increase<sup>151-152</sup>. Guo *et al.*<sup>153</sup> also observed the transport properties of H-Si nanowires were strongly influenced by the presence of adsorbates, such as atmospheric water, which facilitate charge transfer to the Si-H bond, resulting in increased conductivity.

Haight *et al.*<sup>85</sup> functionalised H-Si nanowires with phenyl terpyridine (TP) using arenediazonium salts and observed that the electrical properties of Si nanowires could be altered by manipulating the pyridine groups. Surface modification with TP gave rise to a large drop in the conductivity, relative to H-termination, as shown in figure 9(a). The TP-Si nanowires were then exposed to HCl and the conductivity increased beyond that of H-Si nanowires. Following a rinse with base solution ( $\text{NH}_4\text{OH}$ ), the conductivity returned to the original TP-Si nanowire level. The authors used single nanowire XPS to probe the Si nanowire band gap. The spectra in figure 9(b) show that TP-functionalisation resulted in a shift of 260 meV to high binding energies due to charge transfer from TP molecules to Si nanowire, which shifts the Fermi level ( $E_F$ ) towards the CB. This shift in  $E_F$  can be thought of as effectively ‘*n*-doping’ the Si nanowire by TP-functionalisation. Following HCl exposure, the emission spectra is shifted back by 200 meV due to a change in the surface dipole as illustrated in figure 7(b).

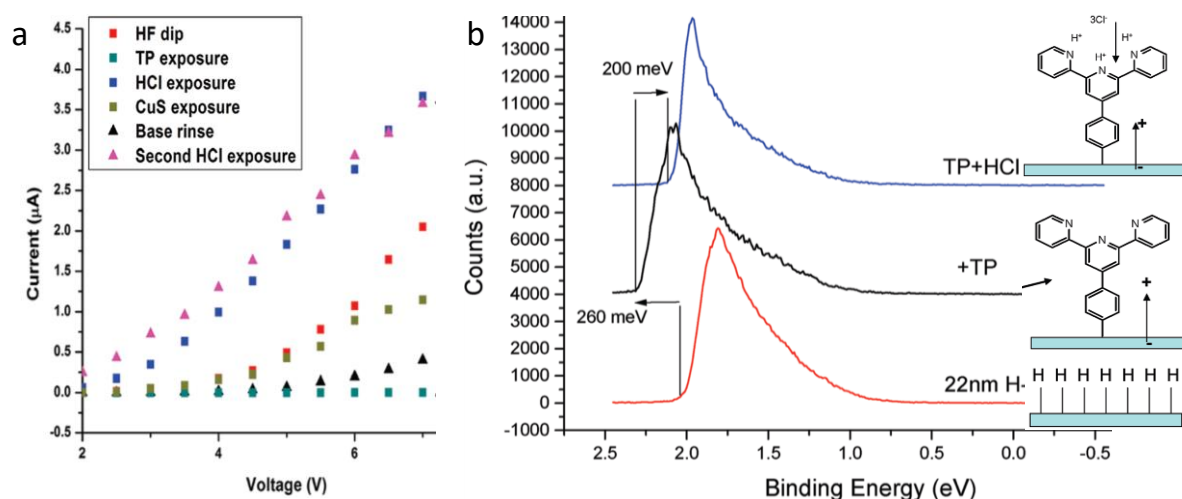


**Figure 9.** (a) Current versus voltage ( $V_{SD}$ ) of Si nanowires with various surface modifications. (b) Photoelectron spectra of single Si nanowires with H-, TP and TP+HCl surface terminations, which are also shown schematically. The arrows indicate the induced dipoles<sup>85</sup>. Reprinted with permission from reference 85. Copyright 2009, American Chemical Society.

The effectiveness and versatility of the surface doping mechanism has recently been demonstrated by Lee and co-workers<sup>154</sup> where the conductivity of Si nanowires could be reversibly tuned from  $p^+p$ -intrinsic- $n-n^+$ , simply by changing the nature of the passivating species. To obtain  $p^+$ -conductivity, H-terminated  $p$ -type Si nanowires were exposed to acidic medium such as acetic acid vapours or  $\text{NO}_2$  gas. The time required for saturation of the surface varied depending on the reagent but all acid-passivated Si nanowires resulted in an increase in the conductivity by more than 4 orders of magnitude, as shown in figure 10(a). Figure 10(b) shows the  $V_g$  dependence of the  $I_{DS}$ - $V_{DS}$  curves with conductance increasing with decreasing positive  $V_g$ , characteristic of  $p$ -type conductivity. Importantly, the transport properties of the original, post-treated Si nanowires could be recovered by  $\text{N}_2/\text{Ar}$  purging, which resulted in the desorption of the surface passivation species. For Si nanowires treated with basic reagents ( $\text{NH}_3$ ), there was an initial drop in the conductivity, followed by a sharp increase in the conductivity as illustrated in figures 10(c)-(e). The initial exposure to  $\text{NH}_3$

consumes holes present at the H-Si nanowire surface, resulting in a drop in conductivity and an effective conversion from *p*-type to intrinsic Si. As the concentration of NH<sub>3</sub> increases further, the electrons injected by NH<sub>3</sub> becomes the dominate charge carrier and the conductivity increases, marking the change to *n*-type Si<sup>155</sup>. DFT calculations have shown NH<sub>3</sub> adsorption on Si nanowires provides a shallow donor states close to the Si CB edge<sup>156</sup>. Surface transfer doping is a potentially attractive alternative to *in-situ* doping methods, where the presence of some dopant precursors, *e.g.* diborane (B<sub>2</sub>H<sub>6</sub>), negatively impact on the morphology of Si and Ge nanowires<sup>157-160</sup>.

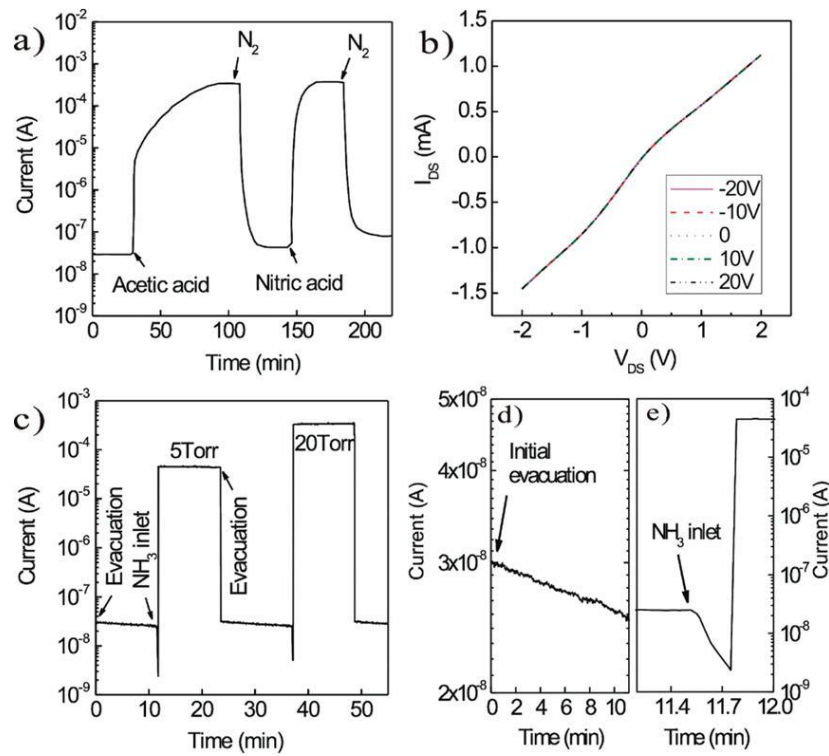


**Figure 10.** (a) Time dependence of  $I_{DS}$  of acid-passivated Si nanowires, measured in air at  $V_{DS} = 2$  V. (b) Gate dependence of  $I_{DS}/V_{DS}$  curves after acid-treatment. (c-e) Time dependence of  $I_{DS}$  of NH<sub>3</sub> passivated Si nanowires, measured in vacuum, air at  $V_{DS} = 2$  V<sup>154</sup>. Reprinted with permission from reference 150. Copyright 2010, American Chemical Society.

The use of surface functionalisation for doping 2D and nanostructured Si has been exploited by Javey and co-workers employing a different strategy, namely molecular layer doping<sup>161</sup>. The H-Si surface is first functionalised with self assembled monolayers containing the dopant species, such as organo-boron or organo-phosphorus ligands. A SiO<sub>2</sub> capping layer is deposited by electron beam evaporation, followed by rapid thermal annealing (RTA), which results in the diffusion of dopant atoms into the Si lattice. Altering the dopant precursor concentration, the RTA time and temperature allows different dopant profiles to be obtained, making this controlled approach an attractive route for the controlled doping of Si and Ge.

### *6.3 Photoinduced Charge Transfer in Si Nanowires*

Photoinduced charge transfer has been studied in semiconductor and carbon nanotube systems, due to the potential to act as optical switches. Winklenmann and co-workers<sup>162</sup> studied the transfer properties of porphyrin-coated *n*-type Si NW FETs. Under dark conditions, a conductance drop relative to untreated nanowires (black curve, figure 11 (a)), was observed after surface modification (blue dashed curve figure 11(a)), which can be attributed to the ground state hole transfer from the porphyrin to the nanowire. On illumination with white light ( $\sim 100 \text{ W m}^{-2}$ ), the conductance was found to increase (solid blue curve, figure 11(a)) due to tunnelling of negative charge from the porphyrin to the nanowire, partially cancelling the reduced gating effect under dark conditions. The effect of enhanced conductivity under illumination was reproducible, as shown in figure 11(b). Furthermore, the transfer properties also exhibited gate voltage dependence, with on/off switching ratios increasing with decreasing  $V_g$ .

Lin *et al.*<sup>163</sup> studied the effect of UV light on APTES-functionalised Si nanowires and found that while *p*-type nanowires displayed a decrease in the resistance with UV illumination, *n*-

type nanowires exhibited an increase in resistance. The surprising observation of enhanced resistance for *n*-type nanowires originates from two competing effects of UV exposure. Firstly, UV illumination excites additional charge carriers in the nanowire, resulting in decreased resistance. The second influence of UV radiation is to induce polarisation of the APTES-functionalisation layers, producing negative surface charges that can accumulate (*p*-type) or deplete (*n*-type) charge carriers in the nanowire. For *p*-type nanowires, both effects work to decrease the resistance, however for *n*-type nanowires the change in resistance is dependent on the strength of the UV-induced APTES polarisation; when APTES dipoles are collectively aligned, the polarisation effects dominate over the UV-induced charge carriers, giving rise to increased resistance.

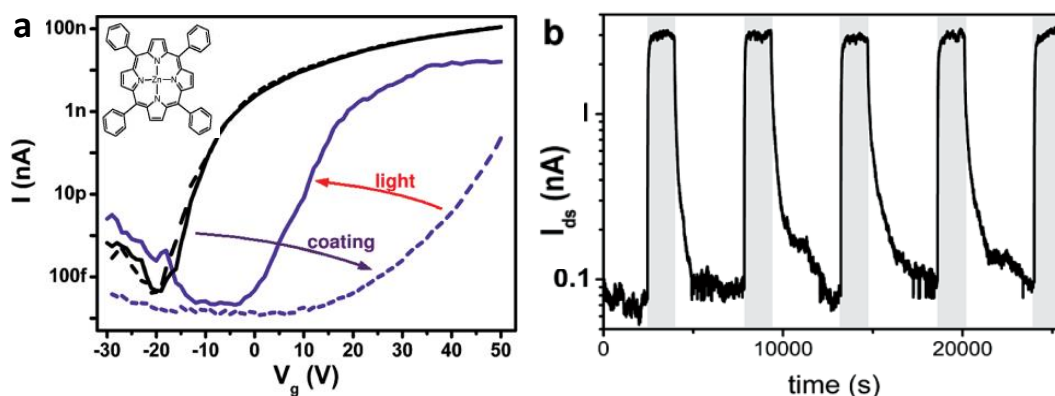


**Figure 11.** (a) Current versus gate voltage of Si nanowires before (black curves) and after porphyrin coating (purple curves). The dashed curves represent values obtained in the dark, continuous curves represent values obtained under white light illumination. (b) Drain-source current ( $I_{DS}$ ) of porphyrin coated Si NW FET as a function of time. The grey shaded areas illustrate the enhanced conductance under illumination conditions<sup>162</sup>. Reproduced with permission from reference 162. Copyright 2010, American Chemical Society.

## 7. Sensing Applications of Functionalised Si and Ge Nanowires



Electrical detection using nanowires configured as FETs is based on evaluating the change in the nanowire electrical properties induced when a target species binds to recognition receptor ligands linked to the nanowire surface. The reduced dimensionality of nanowires implies that changes in the surface potential or surface charge, induced by this target-receptor interaction, affect a significant portion of the nanowire cross-sectional area, resulting in considerably greater sensitivity compared to planar devices<sup>164</sup>. Furthermore, the high surface area to volume ratios of nanowires facilitates a high density of receptor binding sites on the nanowire surface.

Lieber and co-workers<sup>165</sup> demonstrated the fabrication of a Si NW-FET nanosensor for real-time pH detection, shown in figures 12(a) and (b). Oxygen plasma cleaned *p*-type Si nanowires were treated with ATPES to yield a mixed amine ( $-\text{NH}_2$ ) and hydroxyl ( $-\text{OH}$ ) terminated Si surface. Under low pH, protonation of the  $-\text{NH}_2$  groups ( $\text{pK}_a \sim 10$ ) created positive surface charges, causing the depletion of hole carriers and consequently the conductance decreased. Conversely, at high pH, deprotonation of the surface silyl groups to  $\text{SiO}^-$  ( $\text{pK}_a \sim 4\text{-}5$ ), produces a negative gate bias and an accumulation of hole carriers, leading to an increase in the conductance. The conductance displayed a linear pH relationship and is constant for a given pH, as shown in figures 12(c) and (d), respectively. Early reports of nanowire sensors used individual nanowires synthesised by bottom-up processes, such as CVD, making it difficult to control nanowire dimensions. Developments in lithography methods have facilitated the fabrication of high quality Si NW-FETs with excellent diameter control. Due to compatibility with current processing and the ease of fabrication of Si based devices, Si has far exceeded Ge as the material for nanowire sensors, however, Koto *et al.*<sup>166</sup> have demonstrated the successful fabrication of Ge nanowire sensor arrays for pH detection. Si nanowire sensors have been developed for the detection of a broad range of species, some of which are discussed in the following sections.

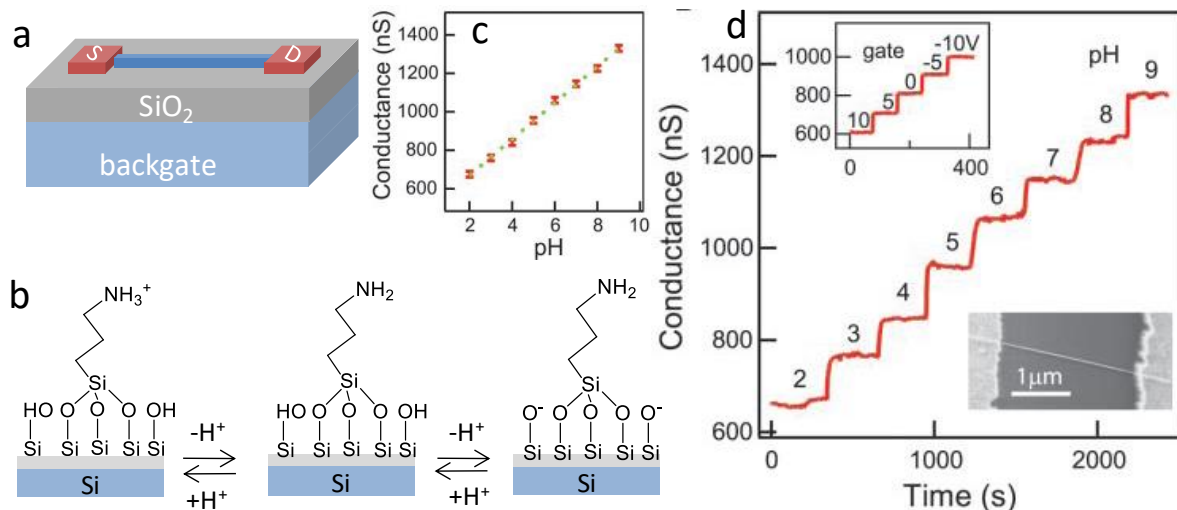


**Figure 12.** (a) Si nanowire FET configured as a pH nanosensor. (b) Surface modification of APTES functionalized Si nanowires on exposure to basic and acid conditions. (c) Conductance versus pH and (d) real time detection of conductance changes for APTES-Si nanowires for pH values ranging from 2 – 9. The inset plot shows the time dependent conductance as a function of  $V_g$ . The inset image displays an SEM image of the Si nanowire device<sup>165</sup>. Reprinted with permission from reference 165. Copyright 2001, AAAS.

### 7.1 Si Nanowire Sensors for the Detection of Biomolecules

Many conventional sensing methods rely on labelling such as fluorescent tags, however Si nanowire based sensors offer the ability of rapid, low cost and real-time monitoring of small biomolecules, proteins and nucleic acids. Wang and co-workers<sup>167</sup> investigated molecular inhibitors to tyrosine kinases using Si nanowires modified with Abl, a protein tyrosine kinase implicated in chronic myelogenous leukemia. The modified Si nanowires were used to investigate the competitive inhibition of ATP binding with organic molecules, such as the drug Gleevec. The conductance was found to decrease with increasing Gleevec concentration as these neutral molecules competitively inhibit the binding of negatively charged ATP at the Abl receptor sites. Si nanowire sensors represent a rapid assay to

investigate the inhibition processes of small-molecules with biomolecules, which has enormous potential for drug discovery and development. Lin and co-workers<sup>168</sup> fabricated dopamine nanosensors using polycrystalline Si nanowire FETs with detection limits in the femtomolar (fM) concentration range obtainable. Dopamine molecules were immobilised through a phenylboronic ester complex, formed by coupling 4-carboxyphenylboronic acid to an APTES modified Si surface.

The first protein detected using Si nanowire FET sensors was streptavidin, using biotin-modified Si nanowires, with detection limits of 10 pM<sup>165</sup>. Since then, real-time detection of various protein markers associated with a number of diseases such as biomarkers for cancer<sup>169-171</sup> and cardiovascular diseases<sup>172-173</sup> has been achieved. Zheng *et al.*<sup>169</sup> used *p*- and *n*-type Si nanowire arrays for multiplexed electrical detection of prostate specific antigen, obtaining detection limits down to 0.9 pg ml<sup>-1</sup>, in undiluted serum. Pui and co-workers<sup>174</sup> immobilised leptin and resistin antibodies via aldehyde-modified Si nanowires for the parallel detection of leptin and resistin adipocytokines. Functionalised Si nanowires can not only be used for the detection of biomolecules but also for cell separation. Kim *et al.*<sup>175</sup> devised streptavidin-functionalised Si nanowire arrays to isolate biotinylated CD4<sup>+</sup> lymphocytes from a heterogeneous mixture of cells, with ~88 % purity.

The ability to employ Si nanowires as nucleic acid bases biosensors has important implications for medical diagnostics. DNA-functionalised Si nanowire FETs have been utilised for the label-free detection of oligonucleotides including the detection of virus DNA<sup>168,176-178</sup>. A major drawback associated with the DNA/DNA sensing mechanism is reduced sensitivity due to electrostatic hindrance from the negatively charged DNA strands. Peptide nucleic acid (PNA) provides an attractive alternative as a receptor for DNA detection as this

neutral molecule exhibits a higher affinity and greater stability than their DNA analogues<sup>96,179-180</sup>. PNA-functionalised Si nanowire sensors display higher sensitivity compared to DNA-modified devices with detection limits for DNA hybridization in the of tens of femtomolar (fM) range<sup>179,181-182</sup>. Recently, Zhang *et al.*<sup>183</sup> prepared morpholino-modified Si nanowire FETs for label-free DNA detection. The morpholino receptors consisted of a nucleobase chain, a non-ionic phosphorodiamidate group bonded to a 6-membered morpholine ring. DNA concentrations of 100 fM could be detected, which constitutes a 3 order of magnitude enhancement in the sensitivity relative to DNA-modified Si nanowires sensors.

## 7.2 Functionalized Si Nanowires for Metal Ion Detection

Table 3 illustrates the nanowire surface modifications utilised for metal ion detection. Zhang and co workers<sup>184</sup> immobilised crown ethers on Si nanowires for Na<sup>+</sup> and K<sup>+</sup> ion detection. The effectiveness of crown ethers as receptors is based in their ability to selectively complex metal ions depending on the size of the crown cavity, a feature which has been exploited for bulk sensing devices. CMOS-compatible *n*-type Si nanowires with a diameter of 30 nm were fabricated by UV lithography. H-terminated Si nanowires were first functionalised with an amino-terminated chain by hydrosilylation of a *t*-BOC protected amine. Glutaraldehyde was employed as a bifunctional linker, to immobilise the amine modified crown ethers; 15-crown-5 and 18-crown-6 were used for Na<sup>+</sup> and K<sup>+</sup> detection, respectively. After binding of the alkali metal ions a large positive charge resides on the surface of the Si nanowires, which increases charge carrier concentration and consequently lowers the measured resistance by ~20 %. The Si nanowire sensor displayed a sensitivity increase of more than 3 orders of magnitude greater than conventional crown ether based sensors with detection limits of 50 nM.

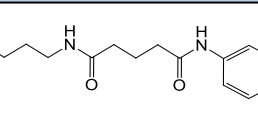
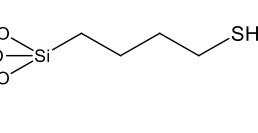
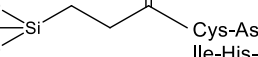
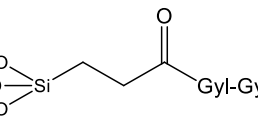
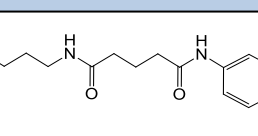
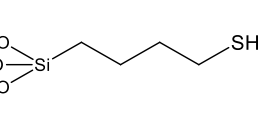
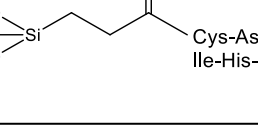
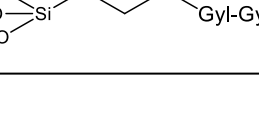
Cui *et al.*<sup>165</sup> used the calcium-binding protein, calmodulin, as receptor molecules for  $\text{Ca}^{2+}$  ions and while the device displayed high selectivity, poor stability can be a drawback associated with protein-based recognition species. Bi *et al.*<sup>185</sup> utilised the phosphate-containing amino acid, phosphotyrosine (p-Try), for  $\text{Ca}^{2+}$  detection. The p-Try residues were introduced by first functionalising lithography fabricated Si nanowire arrays with N-(2-aminoethyl)-3-(trimethoxysilyl)propylamine (AEAPS), which was further reacted with glutaraldehyde to yield an aldehyde-terminated surface. The p-Try was immobilised through a Schiff base reaction and finally reduced to give a secondary amine. Lin *et al.*<sup>172</sup> designed a Si nanowire sensor based on the reversible association between glutathione (GSH) and glutathione S-transferase (GST) for the detection of  $\text{Ca}^{2+}$  and the calmodulin-intetracting protein cardiac troponin I (TnI), a biomarker for myocardial infarction. GSH was immobilised onto APTMS functionalised Si nanowires using a maleimidobenzoyl hydroxylsuccinimide (MBS) bifunctional cross-linker. GST-tagged CaM could be reversibly immobilised allowing for the detection of  $\text{Ca}^{2+}$  ( $>1\ \mu\text{M}$ ) and TnI (7 nM).

Surface functionalisation using metal-selective oligo-peptides have been used for the detection of  $\text{Pb}^{2+}$  and  $\text{Cu}^{2+}$  ions<sup>186-187</sup>. Si nanowires synthesised by chemical etching of Si wafers and functionalised with mercaptopropyltriethoxysilane (MPTES) were used for the detection of heavy metal ions ( $\text{Hg}^{2+}$ ,  $\text{Cd}^{2+}$ )<sup>188</sup>. The functionalised nanowires exhibited concentration-dependent increases in conductivity with increasing ion concentration up to  $10^{-3}\ \text{M}$  and detection limits of  $10^{-7}\ \text{M}$  and  $10^{-4}\ \text{M}$  for  $\text{Hg}^{2+}$  and  $\text{Cd}^{2+}$ , respectively.

Nanowire sensors reported here so far are based on electrical detection of target analytes, Mu and co-workers<sup>189</sup> used 8-aminoquinoline-functionalised Si nanowires for the optical detection of  $\text{Cu}^{2+}$  ions. Si nanowires, grown by thermal evaporation, were functionalised with N-(quinoline-8-yl)-2-(3-triethoxysilyl-propylamino)-acetamide (QIOEt) and then dispersed in a buffered 30 % ethanolic aqueous solution. These solutions were titrated

against various metal ions and their fluorescence properties were monitored. The functionalised nanowires were highly selective towards  $\text{Cu}^{2+}$  species and the fluorescence intensity decreased with increasing  $\text{Cu}^{2+}$  concentration up to 20  $\mu\text{M}$ . Significantly, QIOEt-modified Si nanowires display a higher fluorescence quantum yield compared to QIOEt alone, consequently the functionalised Si nanowires could obtain  $\text{Cu}^{2+}$  detection limits of  $10^{-8}$  M, compared to  $10^{-6}$  M for QIOEt. Furthermore, the Si nanowire fluorescence sensor was reversible by the addition of acid to remove the bound  $\text{Cu}^{2+}$  species, followed by filtration to recover the QIOEt-modified Si nanowires.

**Table 3.** Surface functionalisation of Si nanowire sensors for metal ion detection.

Ion	Functionalisation	Ion	Functionalisation
Na <sup>+</sup> K <sup>+</sup>	 <p>18-crown-6 for K<sup>+</sup></p>	Ca <sup>2+</sup>	
Hg <sup>+</sup> Cd <sup>2+</sup>		Ca <sup>2+</sup>	
Pb <sup>2+</sup>		Ca <sup>2+</sup>	
Cu <sup>2+</sup>		Ca <sup>2+</sup>	

### 7.3 Non-Biological Sensing Applications of Functionalised Si Nanowires

Advancements in Si nanowire-based sensors has been largely focused on the detection of biologically relevant molecules but there has been increasing interest in developing rapid

sensing methods for anti-terrorist applications. Engel *et al.*<sup>190</sup> recently demonstrated that Si nanowire arrays can be used for the ultra-sensitive detection of explosives. The electrical conductance of APES-functionalised Si nanowires is strongly influenced by the presence of 2,4,6-trinitrotoluene (TNT), allowing for detection limits in the sub-femtomolar ( $< 10^{-15}$  M) regime to be obtained. The impressive sensitivities originate from the strong acid-base pairing interaction of the electron-deficient aromatic ring of TNT molecules with the electron-rich amino groups on the APES ligands. The device showed excellent reversibility with conductivity returning to the baseline reading after washing with DI water. Simonato and co-workers<sup>191</sup> devised Si nanoribbon FETs for sub-ppm detection of organophosphorus (OP) molecules, which are used as chemical weapons such as sarin. The receptor ligand consisted of a tertiary amine in close proximity to a primary alcohol, which after interaction with OP molecules, reacted to form a quaternary ammonium salt and phosphate ester.

#### *7.4 Factors Influencing Nanowire Sensor Performance*

Many Si nanowire-based sensors utilise siloxane functionalisation layers with organo-silanes grafted onto the silicon oxide surface. While the siloxane chemistry has the advantages of using many commercially available precursors, this functionalisation approach can lead to multilayer formation and is also dependent on the density of surface hydroxyl groups (-OH) to ensure good surface coverage<sup>192</sup>. Cattani-Scholz and co-workers<sup>96</sup> employed organophosphonates to form self-assembled monolayers on oxidised silicon nanowires. Gu *et al.*<sup>193</sup> reported a Si nanowire nanogap FET sensor for the detection of avian flu; one advantage of the design was the use of silica binding proteins (SBP), which anisotropically immobilise onto silica surfaces without prior need for surface functionalisation such as silylation. The SBP also binds the bioreceptor molecule, in this case the avian influenza

antigen (AI-an). The immobilised SBP-AIa can then be utilised to detect the specific target antibody against AI, *i.e.* anti-AI.

A further issue associated with chemical attachment through the native oxide is that it does not allow for selective binding to the nanowire, but instead functionalises the entire substrate surface, which is typically SiO<sub>2</sub>, thus considerably reducing the sensitivity of the device. Park *et al.*<sup>194</sup> devised a strategy for the selective functionalisation of oxidised Si nanowires using localised nanoscale Joule heating under applied electrical bias. The localised heating ablates a protective polymer layer, polytetrafluoroethylene (PTFE), exposing the nanowire surface, which can then be selectively functionalised with the desired ligands, as illustrated in figure 13(a). Figure 13(b) displays the temperature profile of Si nanowire arrays showing large temperature gradients which enable controlled ablation of the polymer coating.

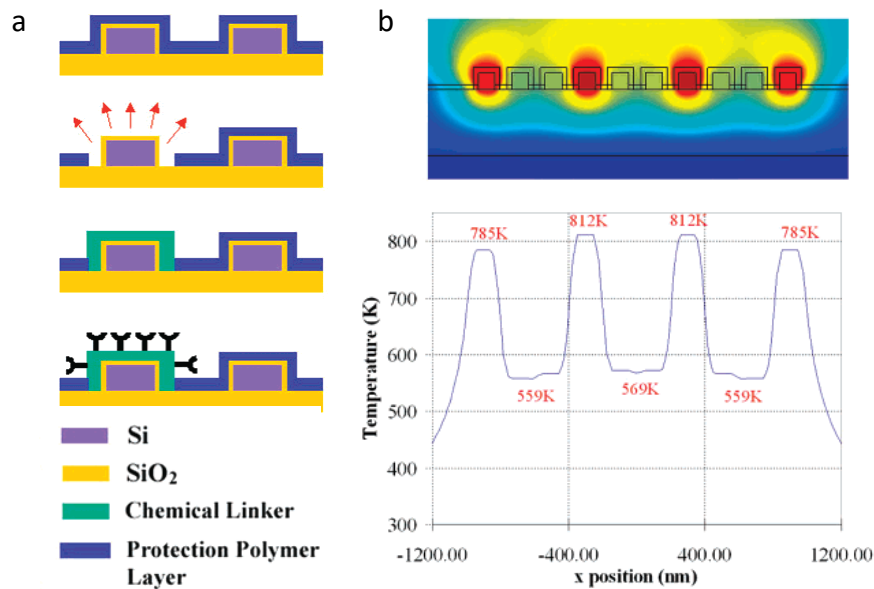


**Figure 13.** (a) Process flow for selective functionalisation of Si nanowires by nanoscale Joule heating. Schematic illustrates (i) deposition of the polymer (PTFE) layer, (ii) localised heating to remove PTFE followed by O<sub>2</sub> plasma treatment, (iii) localised functionalisation with linker molecules and (iv) attachment of desired ligands. (b) Numerical simulation of



temperature distribution in Si nanowire arrays subjected to nanoscale heating using 12 V bias<sup>194</sup>. Reprinted with permission from reference 194. Copyright 2007, American Chemical Society.

These functionalisation methods however, still graft molecules onto the surface oxide and not directly onto the Si surface. The presence of an oxide at the nanowire/organic interface acts as a dielectric making the nanowire less sensitive to charge variations induced by receptor/analyte interactions. Bunimovich *et al.*<sup>178</sup> compared the performance of oxidised and non-oxidised Si nanowires for DNA sensing. Nanowires functionalised via UV-initiated hydrosilylation exhibited enhanced FET characteristics and an order of 2 magnitude increase in the sensitivity of the Si nanowires towards single-strand DNA. Masood and co-workers<sup>195</sup> fabricated Si FET sensors based on nanowires with triangular cross sections having {111} surface facets, which were selectively functionalised by hydrosilylation. The use of {111} surfaces is advantageous as alkylation on Si(111) yields higher quality Si-C monolayers with low surface trap densities relative to other Si surfaces.

The nature of chemical grafting to nanowire surfaces plays a key role in determining performance nanowire based sensors, but several factors influence nano-sensor sensitivity and detection limits. As expected, the sensitivity can be increased with decreasing nanowire diameter<sup>164</sup>, however the nanowire size is limited by lithography and down-sizing also rises the cost of device fabrication. Ahn *et al.*<sup>196</sup> used a double gate Si nanowire FET sensor that showed improved sensitivity compared to the conventional single gate devices. The presence of a secondary gate (G2) allowed the conduction path in the nanowire to be independently controlled. By applying a positive bias to G2 ( $V_{G2} = 0.5$  V), the threshold voltage increased, making the device more sensitive to the presence of charged molecules on the nanowire surface.

Gao *et al.*<sup>197</sup> investigated different operational modes to of Si nanowire FETs and found the sensitivity to be strongly dependent on carrier screening length of Si ( $\lambda_{Si}$ ), taken to be  $\sim 1-2$  nm for a hole density of  $\sim 10^{18}-10^{19} \text{ cm}^{-3}$ , and the nanowire radius ( $R$ ). In a high carrier concentration regime, where  $\lambda_{Si} \ll R$ , the nanowire FET conductance ( $G$ ) varies linearly with  $V_g$ . In a low carrier concentration regime, where  $\lambda_{Si} \gg R$ , the device works in a depleted or subthreshold regime, where  $G$  varies exponentially with  $V_g$ . The longer carrier screening length relative to the nanowire radius means that the surface charges can gate the whole nanowire cross-section, leading to improved sensitivity and lower detection limits<sup>198</sup>. The authors experimentally demonstrated that Si nanowire FET sensors displayed a 500-fold increase in protein detection limits when operated in a depleted mode relative to a linear regime.

A fundamental challenge for the integration of nanowire biosensors stems from the complex make-up of physiological fluids, where factors such as high salt concentration, non-specific binding and biofouling can be problematic. Stern *et al.*<sup>170</sup> fabricated a Si nano-sensor that incorporates a microfluidic purification chip (MPC) and enables analysis from whole blood. The role of the avidin-functionalised MCP is to first capture the desired biomarkers from blood through antibody-DNA binding. After washing, the device is filled with sensing buffers and then irradiated with UV light, resulting in the cleavage of a photolabile group that binds the biomarker-antibody-DNA complex. The contents of the MPC are then transferred to the sensor device consisting of Si nano-ribbons functionalised with secondary antibodies. Biomarker detection requires the binding of 2 antibody receptors, thereby improving selectivity and reducing the detection error. Successful utilisation of this two-step purification-sensing approach is highly promising for the integration of Si nanowire based sensors for medical diagnostics.

## Conclusions

Several strategies have been devised for the formation of robust organic monolayers on Si and Ge nanowires. Organic functionalisation layers provide an effective barrier to prevent surface re-oxidation and enhance electrical performance of Si and Ge nano-electronic devices. The report by Lieber and Cui in 2001<sup>165</sup> on the first Si nanowire sensor, sparked huge interest into the area of nano-sensing and there have been rapid advances in the fabrication of such devices. The low dimensionality of nanowires makes their transport properties highly responsive to processes occurring at the surface and allows for ultrasensitive detection of target molecules. Many challenges remain with regard to the full integration of nanowire based sensors; degradation of the functionalisation layer will significantly reduce the sensing capabilities and the long-term stability of nanowire sensors is not often reported. Furthermore, for highly selective detection of biomolecules in physiological fluids to be realised, functionalisation with more complex assemblies is required. Despite these challenges, there are many potential opportunities for functionalised Si and Ge nanowires such as biocompatible implantable devices for *in vivo* monitoring, lab-on-chip devices and targeted drug delivery.

Grafting organic molecules onto the Si/Ge interface to alter transport properties could provide an entirely different approach to conventional doping of semiconductor nanowires. Further studies into the mechanism of how molecules induce changes to the transport properties, through charge transfer, surface states, and molecular gating effects is essential. A key issue to future applications is the stability of these molecular gates under device operational conditions. Fully elucidating the role of molecular modification has huge potential for nano-electronics such as improved FET performance and molecular memory storage devices. While an enormous understanding of Si and Ge nanowire functionalisation can be gained from the considerable work on 2D surfaces, nanowires also possess fundamental differences and are inherently more complex systems than their bulk counterparts. Understanding the

role nanowire curvature, surface facets, doping, the effect of the growth catalyst and how these factors influence surface reactivity and stability on nanowires will enable selection of the optimal nanowire modification to meet specific applications.

## Acknowledgements

Financial support from the Irish Research Council for Science and Engineering Technology (IRCSET) and Science Foundation Ireland (Grant 08/CE/I1432) is gratefully acknowledged.

## References

- 1 A. M. Morales and C. M. Lieber, *Science*, 1998, **279**, 208.
- 2 P. R. Bandaru and P. Pichanusakorn, *Semicond. Sci. Technol.*, 2010, **25**, 024003.
- 3 Y. Ke, X. J. Weng, J. M. Redwing, C. M. Eichfeld, T. R. Swisher, S. E. Mohny and Y. M. Habib, *Nano Lett.*, 2009, **9**, 4494.
- 4 X. H. Sun, C. Didychuk, T. K. Sham and N. B. Wong, *Nanotechnology*, 2006, **17**, 2925.
- 5 A. T. Heitsch, D. D. Fanfair, H. Y. Tuan and B. A. Korgel, *J. Am. Chem. Soc.*, 2008, **130**, 5436.
- 6 A. M. Chockla and B. A. Korgel, *J. Mater. Chem.*, 2009, **19**, 996.
- 7 A. T. Heitsch, C. M. Hessel, V. A. Akhavan and B. A. Korgel, *Nano Lett.*, 2009, **9**, 3042.
- 8 J. D. Holmes, K. P. Johnston, C. Doty and B. A. Korgel, *Science*, 2000, **287**, 1471.
- 9 X. M. Lu, T. Hanrath, K. P. Johnston and B. A. Korgel, *Nano Lett.*, 2003, **3**, 93.
- 10 T. Hanrath and B. A. Korgel, *J. Am. Chem. Soc.*, 2002, **124**, 1424.
- 11 G. Collins, M. Kolesnik, V. Krstic and J. D. Holmes, *Chem. Mater.*, 2010, **22**, 5235.
- 12 T. Hanrath and B. A. Korgel, *Adv. Mater.*, 2003, **15**, 437.
- 13 H.-Y. Tuan, D. C. Lee and B. A. Korgel, *Angew. Chem. Int. Ed.*, 2006, **45**, 5184.
- 14 H.-Y. Tuan, D. C. Lee, T. Hanrath and B. A. Korgel, *Chem. Mater.*, 2005, **17**, 5705.
- 15 H.-Y. Tuan, D. C. Lee, T. Hanrath and B. A. Korgel, *Nano Lett.*, 2005, **5**, 681.
- 16 R. Q. Zhang, Y. Lifshitz and S. T. Lee, *Adv. Mater.*, 2003, **15**, 635.
- 17 Y. F. Zhang, Y. H. Tang, N. Wang, C. S. Lee, I. Bello and S. T. Lee, *Phys. Rev. B*, 2000, **61**, 4518.
- 18 N. Wang, Y. H. Tang, Y. F. Zhang, C. S. Lee and S. T. Lee, *Phys. Rev. B*, 1998, **58**, 16024.
- 19 F. Tao, S. L. Bernasek and G. Q. Xu, *Chem. Rev.*, 2009, **109**, 3991.
- 20 D. D. M. Wayner and R. A. Wolkow, *J. Chem. Soc.-Perkin Trans. 2*, 2002, 23.
- 21 H. N. Waltenberg and J. T. Yates, *Chem. Rev.*, 1995, **95**, 1589.
- 22 K. A. Perrine and A. V. Teplyakov, *Chem. Soc. Rev.*, 2010, **39**, 3256.
- 23 C. C. Buttner and M. Zacharias, *Appl. Phys. Lett.*, 2006, **89**.
- 24 B. Z. Liu, Y. F. Wang, T. T. Ho, K. K. Lew, S. M. Eichfeld, J. M. Redwing, T. S. Mayer and S. E. Mohny, *J. Vac. Sci. & Technol. A*, 2008, **26**, 370.
- 25 S. Krylyuk, A. V. Davydov, I. Levin, A. Motayed and M. D. Vaudin, *Appl. Phys. Lett.*, 2009, **94**.

- 26 D. B. Kao, J. P. McVittie, W. D. Nix and K. C. Saraswat, *IEEE Trans. Electron Devices*, 1988, **35**, 25.
- 27 D. Shir, B. Z. Liu, A. M. Mohammad, K. K. Lew and S. E. Mohny, *J. Vac. Sci. & Technol. B*, 2006, **24**, 1333.
- 28 T. Xie, V. Schmidt, E. Pippel, S. Senz and U. Gosele, *Small*, 2008, **4**, 64.
- 29 A. Hiraki, M. A. Nicolet and J. W. Mayer, *Appl. Phys. Lett.*, 1971, **18**, 178.
- 30 C. C. Buttner, N. D. Zakharov, E. Pippel, U. Gosele and P. Werner, *Semicond. Sci. Technol.*, 2008, **23**.
- 31 V. A. Sivakov, R. Scholz, F. Syrowatka, F. Falk, U. Gosele and S. H. Christiansen, *Nanotechnology*, 2009, **20**.
- 32 D. Schmeisser, R. D. Schnell, A. Bogen, F. J. Himpsel and D. Rieger, *Surf. Sci.*, 1986, **172**, 455.
- 33 T. Sasada, Y. Nakakita, M. Takenaka and S. Takagi, *J. Appl. Phys.*, 2009, **106**.
- 34 N. Tabet, M. Faiz, N. M. Hamdan and Z. Hussain, *Surf. Sci.*, 2003, **523**, 68.
- 35 K. Prabhakaran and T. Ogino, *Surf. Sci.*, 1995, **325**, 263.
- 36 T. Hanrath and B. A. Korgel, *J. Am. Chem. Soc.*, 2004, **126**, 15466.
- 37 J. Oh and J. C. Campbell, *J. Electronic Mater.*, 2004, **33**, 364.
- 38 S. Sun, Y. Sun, Z. Liu, D. Lee and P. Pianetta, *Appl. Phys. Lett.*, 2006, **89**, 231925.
- 39
- 40 V. Grossi, L. Ottaviano, S. Santucci and M. Passacantando, *J. Non-Cryst. Sol.*, 2010, **356**, 1988.
- 41 D. W. Wang, Y. L. Chang, Q. Wang, J. Cao, D. B. Farmer, R. G. Gordon and H. J. Dai, *J. Am. Chem. Soc.*, 2004, **126**, 11602.
- 42 X. H. Sun, S. D. Wang, N. B. Wong, D. D. D. Ma and S. T. Lee, *Inorg. Chem.*, 2003, **42**, 2398.
- 43 S. Miyazaki, K. Sakamoto, K. Shiba and M. Hirose, *Thin Solid Films*, 1995, **255**, 99.
- 44 K. Choi and J. M. Buriak, *Langmuir*, 2000, **16**, 7737.
- 45 H. Adhikari, P. C. McIntyre, S. Sun, P. Pianetta and C. E. D. Chidsey, *Appl. Phys. Lett.*, 2005, **87**, 263109.
- 46 M. Y. Bashouti, T. Stelzner, S. Christiansen and H. Haick, *J. Phys. Chem. C*, 2009, **113**, 14823.
- 47 S. Rivillon, Y. J. Chabal, L. J. Webb, D. J. Michalak, N. S. Lewis, M. D. Halls and K. Raghavachari, *J. Vac. Sci. Technol. A*, 2005, **23**, 1100.
- 48 A. Bansal, X. L. Li, I. Lauermann, N. S. Lewis, S. I. Yi and W. H. Weinberg, *J. Am. Chem. Soc.*, 1996, **118**, 7225.
- 49 P. G. Cao, H. B. Yu and J. R. Heath, *J. Phys. Chem. B*, 2006, **110**, 23615.
- 50 H. Jagannathan, J. Kim, M. Deal, M. Kelly and Y. Nishi, *ECS Trans.*, 2006, **3**, 1175.
- 51 G. Collins, P. Fleming, S. Barth, C. O'Dwyer, J. J. Boland, M. A. Morris and J. D. Holmes, *Chem. Mat.*, 2010, **22**, 6370.
- 52 P. W. Loscutoff and S. F. Bent, *Annu. Rev. Phys. Chem.*, 2006, **57**, 467.
- 53 J. M. Buriak, *Chem. Rev.*, 2002, **102**, 1271.
- 54 S. Ciampi, J. B. Harper and J. J. Gooding, *Chem. Soc. Rev.*, 2010, **39**, 2158.
- 55 M. R. Linford, P. Fenter, P. M. Eisenberger and C. E. D. Chidsey, *J. Am. Chem. Soc.*, 1995, **117**, 3145.
- 56 A. B. Sieval, A. L. Demirel, J. W. M. Nissink, M. R. Linford, J. H. van der Maas, W. H. de Jeu, H. Zuilhof and E. J. R. Sudholter, *Langmuir*, 1998, **14**, 1759.
- 57 M. M. Sung, G. J. Kluth, O. W. Yauw and R. Maboudian, *Langmuir*, 1997, **13**, 6164.
- 58 A. B. Sieval, V. Vleeming, H. Zuilhof and E. J. R. Sudholter, *Langmuir*, 1999, **15**, 8288.
- 59 R. L. Cicero, M. R. Linford and C. E. D. Chidsey, *Langmuir*, 2000, **16**, 5688.

- 60 F. Effenberger, G. Gotz, B. Bidlingmaier and M. Wezstein, *Angew. Chem.-Int. Ed.*, 1998, **37**, 2462.
- 61 R. Boukherroub and D. D. M. Wayner, *J. Am. Chem. Soc.*, 1999, **121**, 11513.
- 62 A. Langner, A. Panarello, S. Rivillon, O. Vassilyev, J. G. Khinast and Y. J. Chabal, *J. Am. Chem. Soc.*, 2005, **127**, 12798.
- 63 X. Y. Wang, R. E. Ruther, J. A. Streifer and R. J. Hamers, *J. Am. Chem. Soc.*, 2010, **132**, 4048.
- 64 L. Scheres, R. Achten, M. Giesbers, L. de Smet, A. Arafat, E. J. R. Sudholter, A. T. M. Marcelis and H. Zuilhof, *Langmuir*, 2009, **25**, 1529.
- 65 Q. Y. Sun, L. de Smet, B. van Lagen, M. Giesbers, P. C. Thune, J. van Engelenburg, F. A. de Wolf, H. Zuilhof and E. J. R. Sudholter, *J. Am. Chem. Soc.*, 2005, **127**, 2514.
- 66 R. Boukherroub, S. Morin, F. Bensebaa and D. D. M. Wayner, *Langmuir*, 1999, **15**, 3831.
- 67 J. M. Buriak, M. P. Stewart, T. W. Geders, M. J. Allen, H. C. Choi, J. Smith, D. Raftery and L. T. Canham, *J. Am. Chem. Soc.*, 1999, **121**, 11491.
- 68 M. R. Linford and C. E. D. Chidsey, *J. Am. Chem. Soc.*, 1993, **115**, 12631.
- 69 O. Assad, S. R. Puniredd, T. Stelzner, S. Christiansen and H. Haick, *J. Am. Chem. Soc.*, 2008, **130**, 17670.
- 70 E. J. Nemanick, P. T. Hurley, B. S. Brunschwig and N. Lewis, *J. Phys. Chem. B.*, 2006, **110**, 14800.
- 71 A. Bansal, X. L. Li, S. I. Yi, W. H. Weinberg and N. S. Lewis, *J. Phys. Chem. B*, 2001, **105**, 10266.
- 72 M. Y. Bashouti, T. Stelzner, A. Berger, S. Christiansen and H. Haick, *J. Phys. Chem. C.*, 2008, **112**, 19168.
- 73 L. Scheres, M. Giesbers and H. Zuilhof, *Langmuir*, 2010, **26**, 4790.
- 74 Z. R. Scheibal, W. Xu, J. F. Audiffred, J. E. Henry and J. C. Flake, *Electrochem. Solid State Lett.*, 2008, **11**, K81.
- 75 S. S. S. Vegunta, J. N. Ngunjiri, W. Xu and J. C. Flake, *ECS Trans.*, 2010, **25**, 203.
- 76 G. W. Cullen, J. A. Amick and D. Gerlich, *J. Electrochem. Soc.*, 1962, **109**, 124.
- 77 J. He, Z. H. Lu, S. A. Mitchell and D. D. M. Wayner, *J. Am. Chem. Soc.*, 1998, **120**, 2660.
- 78 D. Wang and H. Dai, *Appl. Phys. A.*, 2006, **85**, 217.
- 79 V. C. Holmberg and B. A. Korgel, *Chem. Mat.*, 2010, **22**, 3698.
- 80 D. Wang, Y.-L. Chang, Z. Liu and H. Dai, *J. Am. Chem. Soc.*, 2005, **127**, 11871.
- 81 C. H. deVilleneuve, J. Pinson, M. C. Bernard and P. Allongue, *J. Phys. Chem. B*, 1997, **101**, 2415.
- 82 P. Allongue, C. H. de Villeneuve, J. Pinson, F. Ozanam, J. N. Chazalviel and X. Wallart, *Electrochim. Acta*, 1998, **43**, 2791.
- 83 P. Allongue, C. H. de Villeneuve and J. Pinson, *Electrochim. Acta*, 2000, **45**, 3241.
- 84 M. P. Stewart, F. Maya, D. V. Kosynkin, S. M. Dirk, J. J. Stapleton, C. L. McGuiness, D. L. Allara and J. M. Tour, *J. Am. Chem. Soc.*, 2004, **126**, 370.
- 85 R. Haight, L. Sekaric, A. Afzali and D. Newns, *Nano Lett.*, 2009, **9**, 3165.
- 86 G. Collins, P. Fleming, C. O'Dwyer, M. A. Morris and J. D. Holmes, *Chem. Mat.*, 2011, **23**, 1883.
- 87 A. B. Sieval, R. Linke, G. Heij, G. Meijer, H. Zuilhof and E. J. R. Sudholter, *Langmuir*, 2001, **17**, 7554.
- 88 T. Strother, R. J. Hamers and L. M. Smith, *Nucl. Acid Res.*, 2000, **28**, 3535.
- 89 M. W. Shao, H. Wang, Y. Fu, J. Hua and D. D. D. Ma, *J. Chem. Sci.*, 2009, **121**, 323.
- 90 T. Bocking, A. Salomon, D. Cahen and J. J. Gooding, *Langmuir*, 2007, **23**, 3236.
- 91 J. Pinson and F. Podvorica, *Chem. Soc. Rev.*, 2005, **34**, 429.

- 92 H. C. Kolb, M. G. Finn and K. B. Sharpless, *Angew. Chem.-Int. Ed.*, 2001, **40**, 2004.
- 93 C. Suspene, R. Barattin, C. Celle, A. Carella and J. P. Simonato, *J. Phys. Chem. C*, 2010, **114**, 3924.
- 94 C. Haensch, T. Erdmenger, M. W. M. Fijten, S. Hoepfner and U. S. Schubert, *Langmuir*, 2009, **25**, 8019.
- 95 V. C. Holmberg, M. R. Rasch and B. A. Korgel, *Langmuir*, 2010, **26**, 14241.
- 96 A. Cattani-Scholz, D. Pedone, M. Dubey, S. Neppel, B. Nickel, P. Feulner, J. Schwartz, G. Abstreiter and M. Tarnow, *Acs Nano*, 2008, **2**, 1653.
- 97 J. A. Streifer, H. Kim, B. M. Nichols and R. J. Hamers, *Nanotechnology*, 2005, **16**, 1868.
- 98 C.-P. Li, C. S. Lee, X.-L. Ma, N. Wang, R.-Q. Zhang and S.-T. Lee, *Adv. Mater.*, 2003, **15**, 607.
- 99 T. Hanrath and B. A. Korgel, *Small*, 2005, **1**, 717.
- 100 D. D. D. Ma, C. S. Lee, F. C. K. Au, S. Y. Tong and S. T. Lee, *Science*, 2003, **299**, 1874.
- 101 M. A. Hines, Y. J. Chabal, T. D. Harris and A. L. Harris, *Phys. Rev. Lett.*, 1993, **71**, 2280.
- 102 E. P. Boonekamp, J. J. Kelly, J. Vandeven and A. H. M. Sondag, *J. Appl. Phys.*, 1994, **75**, 8121.
- 103 M. Y. Bashouti, Y. Paska, S. R. Puniredd, T. Stelzner, S. Christiansen and H. Haick, *Phys. Chem. Chem. Phys.*, 2009, **11**, 3845.
- 104 R. Q. Zhang, Y. Lifshitz, D. D. D. Ma, Y. L. Zhao, T. Frauenheim, S. T. Lee and S. Y. Tong, *J. Chem. Phys.*, 2005, **123**.
- 105 T. Deegan and G. Huges, *Appl. Surf. Sci.*, 1998, **123**, 66.
- 106 S. Rivillon, Y. J. Chabal, F. Amy and A. Kahn, *Appl. Phys. Lett.*, 2005, **87**, 253101.
- 107 S. M. Han, R. Ashurt, C. Carraro and M. Roy, *J. Am. Chem. Soc.*, 2001, **123**, 2422.
- 108 B. S. Simpkins, M. A. Mastro, C. R. Eddy and P. E. Pehrsson, *J. Appl. Phys.*, 2008, **103**.
- 109 K. I. Seo, S. Sharma, A. A. Yasseri, D. R. Stewart and T. I. Kamins, *Electrochem. Solid State Lett.*, 2006, **9**, G69.
- 110 I. Kimukin, M. S. Islam and R. S. Williams, *Nanotechnology*, 2006, **17**, S240.
- 111 N. Rochdi, D. Tonneau, F. Jandard, H. Dallaporta and V. Safarov, *Phys. Status Solidi A*, 2008, **205**, 1157.
- 112 H. Haick, P. T. Hurley, A. I. Hochbaum, P. D. Yang and N. S. Lewis, *J. Am. Chem. Soc.*, 2006, **128**, 8990.
- 113 M. Y. Bashouti, R. T. Tung and H. Haick, *Small*, 2009, **5**, 2761.
- 114 Y. Cui, Z. H. Zhong, D. L. Wang, W. U. Wang and C. M. Lieber, *Nano Lett.*, 2003, **3**, 149.
- 115 M. Houssa, E. Chagarov and A. Kummel, *MRS Bull.*, 2009, **34**, 504.
- 116 G. Gu, M. Burghard, G. T. Kim, G. S. Dusberg, P. W. Chiu, V. Krstic and W. Q. Han, *J. Appl. Phys.*, 2001, **90**, 5747.
- 117 T. Hanrath and B. A. Korgel, *J. Phys. Chem. B*, 2005, **109**, 5518.
- 118 R. H. J. Kingston, *J. Appl. Phys.*, 1956, **27**, 101.
- 119 B. Yoo, A. Dodabalapur, D. C. Lee, T. Hanrath and B. A. Korgel, *Appl. Phys. Lett.*, 2007, **90**.
- 120 T. Hanrath and B. A. Korgel, *Proc. IMechE, Part N: J. Nanoengineering and Nanosystems*, 2004, **218**, 25.
- 121 C. Harris and E. P. O'Reilly, *Physica E*, 2006, **32**, 341.
- 122 A. K. Singh, V. Kumar, R. Note and Y. Kawazoe, *Nano Lett.*, 2006, **6**, 920.
- 123 T. Vo, A. J. Williamson and G. Galli, *Phys. Rev. B*, 2006, **74**.

- 124 J. A. Yan, L. Yang and M. Y. Chou, *Phys. Rev. B*, 2007, **76**.
- 125 S. Cahangirov and S. Ciraci, *Phys. Rev. B*, 2009, **80**.
- 126 X. Y. Zhao, C. M. Wei, L. Yang and M. Y. Chou, *Phys. Rev. Lett.*, 2004, **92**.
- 127 D. Medaboina, V. Gade, S. K. R. Patil and S. V. Khare, *Phys. Rev. B*, 2007, **76**.
- 128 P. Logan and X. H. Peng, *Phys. Rev. B*, 2009, **80**.
- 129 A. N. Kholod, V. L. Shaposhnikov, N. Sobolev, V. E. Borisenko, F. A. D'Avitaya and S. Ossicini, *Phys. Rev. B*, 2004, **70**.
- 130 R. Rurali, B. Aradi, T. Frauenheim and A. Gali, *Phys. Rev. B*, 2007, **76**.
- 131 A. J. Lu, R. Q. Zhang and S. T. Lee, *Appl. Phys. Lett.*, 2008, **92**.
- 132 A. Hmiel and Y. Q. Xue, *Phys. Rev. B*, 2009, **80**.
- 133 H. Scheel, S. Reich and C. Thomsen, *Phys. Status Solidi B*, 2005, **242**, 2474.
- 134 M. Bruno, M. Palummo, A. Marini, R. Del Sole, V. Olevano, A. N. Kholod and S. Ossicini, *Phys. Rev. B*, 2005, **72**.
- 135 R. Pekoz and J. Y. Raty, *Phys. Rev. B*, 2009, **80**.
- 136 J. E. Northrup, *Phys. Rev. B*, 1991, **44**, 1419.
- 137 H. Xu, X. H. Zhang and R. Q. Zhang, *Phys. Rev. B*, 2009, **80**.
- 138 P. W. Leu, B. Shan and K. J. Cho, *Phys. Rev. B*, 2006, **73**.
- 139 C. Y. Yeh, S. B. Zhang and A. Zunger, *Phys. Rev. B*, 1994, **50**, 14405.
- 140 M. Nolan, S. O'Callaghan, G. Fagas, J. C. Greer and T. Frauenheim, *Nano Lett.*, 2007, **7**, 34.
- 141 X. D. Xu and P. Servati, *Nano Lett.*, 2009, **9**, 1999.
- 142 M. F. Ng, L. P. Zhou, S. W. Yang, L. Y. Sim, V. B. C. Tan and P. Wu, *Phys. Rev. B*, 2007, **76**.
- 143 B. Aradi, L. E. Ramos, P. Deak, T. Kohler, F. Bechstedt, R. Q. Zhang and T. Frauenheim, *Phys. Rev. B*, 2007, **76**.
- 144 L. Huang, N. Lu, J. A. Yan, M. Y. Chou, C. Z. Wang and K. M. Ho, *J. Phys. Chem. C*, 2008, **112**, 15680.
- 145 A. J. Lu, R. Q. Zhang and S. T. Lee, *Nanotechnology*, 2008, **19**.
- 146 M. F. Ng, L. Y. Sim, H. X. Da, H. M. Jin, K. H. Lim and S. W. Yang, *Theor. Chem. Acc.*, 2010, **127**, 689.
- 147 A. Y. Anagaw, R. A. Wolkow and G. A. DiLabio, *J. Phys. Chem. C*, 2008, **112**, 3780.
- 148 R. Kagimura, R. W. Nunes and H. Chacham, *Phys. Rev. Lett.*, 2007, **98**.
- 149 M. W. Jing, M. Ni, W. Song, J. Lu, Z. X. Gao, L. Lai, W. N. Mei, D. P. Yu, H. Q. Ye and L. Wang, *J. Phys. Chem. B*, 2006, **110**, 18332.
- 150 J. Ristein, *Science*, 2006, **313**, 1057.
- 151 J. S. Jie, W. J. Zhang, K. Q. Peng, G. D. Yuan, C. S. Lee and S. T. Lee, *Adv. Funct. Mater.*, 2008, **18**, 3251.
- 152 S. Miyazaki, J. Schafer, J. Ristein and L. Ley, *Appl. Phys. Lett.*, 1996, **68**, 1247.
- 153 C. S. Guo, L. B. Luo, G. D. Yuan, X. B. Yang, R. Q. Zhang, W. J. Zhang and S. T. Lee, *Angew. Chem.-Int. Ed.*, 2009, **48**, 9896.
- 154 G. D. Yuan, Y. B. Zhou, C. S. Guo, W. J. Zhang, Y. B. Tang, Y. Q. Li, Z. H. Chen, Z. B. He, X. J. Zhang, P. F. Wang, I. Bello, R. Q. Zhang, C. S. Lee and S. T. Lee, *ACS Nano*, 2010, **4**, 3045.
- 155 M. Chiesa, G. Amato, L. Boarino, E. Garrone, F. Geobaldo and E. Giamello, *Angew. Chem.-Int. Ed.*, 2003, **42**, 5032.
- 156 A. Miranda-Duran, X. Cartoixa, M. C. Irisson and R. Rurali, *Nano Lett.*, 2010, **10**, 3590.
- 157 F. Li, P. D. Nellist and D. J. H. Cockayne, *Appl. Phys. Lett.*, 2009, **94**.
- 158 E. Tutuc, J. O. Chu, J. A. Ott and S. Guha, *Appl. Phys. Lett.*, 2006, **89**, 263101.
- 159 E. Tutuc, S. Guha and J. O. Chu, *Appl. Phys. Lett.*, 2006, **88**, 043113.



- 160 C. Y. Meng, B. L. Shih and S. C. Lee, *J. Nanopart. Res.*, 2005, **7**, 615.
- 161 J. C. Ho, R. Yerushalmi, Z. A. Jacobson, Z. Fan, R. L. Alley and A. Javey, *Nature Mater.*, 2008, **7**, 62.
- 162 C. B. Winkelmann, I. Ionica, X. Chevalier, G. Royal, C. Bucher and V. Bouchiat, *Nano Lett.*, 2007, **7**, 1454.
- 163 M. C. Lin, C. J. Chu, L. C. Tsai, H. Y. Lin, C. S. Wu, Y. P. Wu, Y. N. Wu, D. B. Shieh, Y. W. Su and C. D. Chen, *Nano Lett.*, 2007, **7**, 3656.
- 164 N. Elfstrom, R. Juhasz, I. Sychugov, T. Engfeldt, A. E. Karlstrom and J. Linnros, *Nano Lett.*, 2007, **7**, 2608.
- 165 Y. Cui, Q. Q. Wei, H. K. Park and C. M. Lieber, *Science*, 2001, **293**, 1289.
- 166 M. Koto, P. W. Leu and P. C. McIntyre, *J. Electrochem. Soc.*, 2009, **156**, K11.
- 167 W. U. Wang, C. Chen, K. H. Lin, Y. Fang and C. M. Lieber, *Proc. Nat. Acad. Sci.*, 2005, **102**, 3208.
- 168 C. H. Lin, C. Y. Hsiao, C. H. Hung, Y. R. Lo, C. C. Lee, C. J. Su, H. C. Lin, F. H. Ko, T. Y. Huang and Y. S. Yang, *Chem. Comm.*, 2008, 5749.
- 169 G. F. Zheng, F. Patolsky, Y. Cui, W. U. Wang and C. M. Lieber, *Nature Biotechnol.*, 2005, **23**, 1294.
- 170 E. Stern, A. Vacic, N. K. Rajan, J. M. Criscione, J. Park, B. R. Ilic, D. J. Mooney, M. A. Reed and T. M. Fahmy, *Nature Nanotechnol.*, 2010, **5**, 138.
- 171 E. Stern, J. F. Klemic, D. A. Routenberg, P. N. Wyrembak, D. B. Turner-Evans, A. D. Hamilton, D. A. LaVan, T. M. Fahmy and M. A. Reed, *Nature*, 2007, **445**, 519.
- 172 T. W. Lin, P. J. Hsieh, C. L. Lin, Y. Y. Fang, J. X. Yang, C. C. Tsai, P. L. Chiang, C. Y. Pan and Y. T. Chen, *Proc. Nat. Acad. Sci.*, 2010, **107**, 1047.
- 173 J. H. Chua, R. E. Chee, A. Agarwal, S. M. Wong and G. J. Zhang, *Anal. Chem.*, 2009, **81**, 6266.
- 174 T. S. Pui, A. Agarwal, F. Ye, Z. Q. Ton, Y. X. Huang and P. Chen, *Nanoscale*, 2009, **1**, 159.
- 175 S. T. Kim, D. J. Kim, T. J. Kim, D. W. Seo, T. H. Kim, S. Y. Lee, K. Kim, K. M. Lee and S. K. Lee, *Nano Lett.*, 2010, **10**, 2877.
- 176 Z. Li, Y. Chen, X. Li, T. I. Kamins, K. Nauka and R. S. Williams, *Nano Lett.*, 2004, **4**, 245.
- 177 C. C. Wu, F. H. Ko, Y. S. Yang, D. L. Hsia, B. S. Lee and T. S. Su, *Biosens. Bioelectron.*, 2009, **25**, 820.
- 178 Y. L. Bunimovich, Y. S. Shin, W. S. Yeo, M. Amori, G. Kwong and J. R. Heath, *J. Am. Chem. Soc.*, 2006, **128**, 16323.
- 179 J. Hahm and C. M. Lieber, *Nano Lett.*, 2004, **4**, 51.
- 180 G. J. Zhang, G. Zhang, J. H. Chua, R. E. Chee, E. H. Wong, A. Agarwal, K. D. Buddharaju, N. Singh, Z. Q. Gao and N. Balasubramanian, *Nano Lett.*, 2008, **8**, 1066.
- 181 G. J. Zhang, J. H. Chua, R. E. Chee, A. Agarwal and S. M. Wong, *Biosens. Bioelectron.*, 2009, **24**, 2504.
- 182 G. J. Zhang, L. Zhang, M. J. Huang, L. B. Luo, G. K. I. Tay, E. J. A. Lim, T. G. Kang and Y. Chen, *Sens. Actuators B*, 2010, **146**, 138.
- 183 G. J. Zhang, Z. H. H. Luo, M. J. Huang, G. K. I. Tay and E. J. A. Lim, *Biosens. Bioelectron.*, 2010, **25**, 2447.
- 184 G. J. Zhang, A. Agarwal, K. D. Buddharaju, N. Singh and Z. Q. Gao, *Appl. Phys. Lett.*, 2007, **90**.
- 185 X. Y. Bi, W. L. Wong, W. J. Ji, A. Agarwal, N. Balasubramanian and K. L. Yang, *Biosens. Bioelectron.*, 2008, **23**, 1442.
- 186 X. Y. Bi, A. Agarwal, N. Balasubramanian and K. L. Yang, *Electrochem. Comm.*, 2008, **10**, 1868.

- 187 X. Y. Bi, A. Agarwal and K. L. Yang, *Biosens. Bioelectron.*, 2009, **24**, 3248.
- 188 L. B. Luo, J. S. Jie, W. F. Zhang, Z. B. He, J. X. Wang, G. D. Yuan, W. J. Zhang, L. C. M. Wu and S. T. Lee, *Appl. Phys. Lett.*, 2009, **94**.
- 189 L. X. Mu, W. S. Shi, J. C. Chang and S. T. Lee, *Nano Lett.*, 2008, **8**, 104.
- 190 Y. Engel, R. Elnathan, A. Pevzner, G. Davidi, E. Flaxer and F. Patolsky, *Angew. Chem.-Int. Ed.*, 2010, **49**, 6830.
- 191 S. Clavaguera, A. Carella, L. Caillier, C. Celle, J. Pecaut, S. Lenfant, D. Vuillaume and J. P. Simonato, *Angew. Chem.-Int. Ed.*, 2010, **49**, 4063.
- 192 C. Haensch, S. Hoeppener and U. S. Schubert, *Chem. Soc. Rev.*, 2010, **39**, 2323.
- 193 B. Gu, T. J. Park, J. H. Ahn, X. J. Huang, S. Y. Lee and Y. K. Choi, *Small*, 2009, **5**, 2407.
- 194 I. Park, Z. Y. Li, A. P. Pisano and R. S. Williams, *Nano Lett.*, 2007, **7**, 3106.
- 195 M. N. Masood, S. Chen, E. T. Carlen and A. Van den Berg, *ACS Appl. Mater. Inter.*, 2010, **2**, 3422.
- 196 J. H. Ahn, S. J. Choi, J. W. Han, T. J. Park, S. Y. Lee and Y. K. Choi, *Nano Lett.*, 2010, **10**, 2934.
- 197 X. P. A. Gao, G. F. Zheng and C. M. Lieber, *Nano Lett.*, 2010, **10**, 547.
- 198 U. Monga and T. A. Fjeldly, *Phys. Scr.*, 2010, **T141**.